THE ESCAPE OF HIGH-ENERGY PHOTONS FROM GAMMA-RAY BURSTS

Matthew G. Baring[1] and Alice K. Harding
Laboratory for High Energy Astrophysics, Code 661,
NASA Goddard Space Flight Center, Greenbelt, MD 20771, U.S.A.
baring@lheavx.gsfc.nasa.gov, harding@twinkie.gsfc.nasa.gov

ABSTRACT

Eleven bright gamma-ray bursts (GRBs) detected by BATSE have also been seen at much higher energies by EGRET, six at energies above 10 MeV. Most distinctive among these is GRB940217, which includes long duration, hard gamma-ray emission and the most energetic GRB photon detection to date, around 18 GeV. Such observations imply that these bursts are optically thin to photon-photon pair production at all observed energies, for target photons both internal and external to the source. For bursts more than about 30pc away, internal transparency can be achieved only if the source is moving with a relativistic bulk Lorentz factor $\Gamma \gg 1$, or if the radiation is highly beamed. Early calculations of $\gamma\gamma \to e^+e^-$ considerations for GRBs were limited to cases of a beam with opening half-angle $\Theta_{\rm B} \sim 1/\Gamma$, or expansions of infinitely thin spherical shells. This paper presents our extension of pair production optical depth calculations in relativistically expanding sources to more general geometries, including shells of finite thickness and arbitrary opening angle. The problem is reduced analytically to a single integral in the special, but quite broadly applicable case, of observing photons only along the axis of the expansion. We find that the minimum bulk Lorentz factor for the EGRET sources to be optically thin, i.e. display no spectral attenuation, is only moderately dependent on the shell thickness and virtually independent of its opening solid angle if $\Theta_{\rm B} \gtrsim 1/\Gamma$. This insensitivity to $\Theta_{\rm B}$ relieves the commonly-perceived number problem for non-repeating sources at cosmological distances, i.e. it is not necessary to invoke small $\Theta_{\rm B}$ to effect photon escape. The values of Γ obtained, typically of the order of 10 for halo bursts and $\gtrsim 100$ for sources of cosmological origin, depend somewhat on the choice of GRB timescale used to determine the expansion size. Our new limits on required velocity for given source geometries will aid in placing realistic constraints on GRB source models.

Subject headings: radiation mechanisms: misc. — stars: neutron — gamma-rays: bursts — relativity

[1]Compton Fellow, Universities Space Research Association

1. INTRODUCTION

Gamma-ray bursts (GRBs) are the brightest sources in the gamma-ray sky and they may also be among the most distant sources in the Universe. The discovery by the BATSE detector on the Compton Gamma-Ray Observatory (CGRO) that the spatial distribution of GRBs is isotropic and inhomogeneous (Meegan et al. 1992, 1996) suggests that the sources are either in an extended galactic halo or at cosmological distances. The level of isotropy of the GRB spatial distribution limits halo models to core radii of around 50–80 kpc (Hakkila et al. 1995); tighter constraints are expected for more recent data accumulations, and Briggs et al. (1996) suggest that a galactic halo shell distribution must be at least 120 kpc distant. The observed average fluxes of GRBs at Earth therefore imply high luminosities for isotropically emitting sources: $L \simeq 10^{42-43}\,\mathrm{erg\,s^{-1}}$ at a distance of $d = 100$ kpc and $L \simeq 10^{50-51}\,\mathrm{erg\,s^{-1}}$ at a distance of $d = 1$ Gpc. In addition, rapid time variability ($\Delta t \sim$ several ms) is observed in GRB light curves, whose structural diversity is illustrated, for example in the BATSE 1B catalogue in Fishman et al. (1994). This variability implies a compact source size, which in combination with the high luminosities yields photon densities that are high enough to make galactic halo or cosmological GRBs optically thick to photon-photon pair production by many orders of magnitude. One would then expect attenuation of the observed spectrum (perhaps as a quasi-exponential cutoff, trough or shelf: examples are depicted in Baring and Harding 1997) around the pair production threshold of 1 MeV if the GRB sources are more distant than a few kpc and have quasi-isotropic radiation fields (Schmidt 1978, Epstein 1985).

Yet GRB spectra are observed to extend well beyond 1 MeV and into the GeV range. The GRS detector on the SMM satellite first measured emission in GRB spectra significantly above 1 MeV, often extending up to 10 MeV (e.g. Nolan et al. 1983), and in one case up to 80 MeV (Share et al. 1986). BATSE routinely observes GRB spectra extending up to and above 1 MeV. While most bursts exhibit spectral steepening at a variety of energies between 50 keV and few hundred keV (Band et al. 1993; see also Schaefer et al. 1994 for the BATSE 1B spectroscopy catalogue), a number of bursts display spectral breaks between 500 keV and about 2 MeV (Schaefer et al. 1992), but no cutoffs. The EGRET instrument, also on CGRO, has detected emission above 50 MeV from four of the brighter GRBs triggered by BATSE, a fifth up to 30 MeV and another three up to a few MeV; all are consistent with power-law spectra extending to as high as 1.2 GeV, in the case of GRB930131 (Sommer et al. 1994), and 3.4 GeV for GRB940217 (Hurley et al. 1994). The GRB940217 source is best known for exhibiting delayed or prolonged high energy emission, detected 80–100 minutes (i.e. more than one full earth orbit of CGRO) after the initial trigger, including a photon of energy 18 GeV (Hurley et al. 1994) that is not markedly inconsistent with extrapolation of the power-law continuum. In fact, some evidence for delayed high energy emission pre-dated GRB940217, with the observation (Dingus et al. 1994) of a single 10 GeV photon that could have been associated with GRB910503. It is clear that, in contrast to soft gamma-ray repeaters (SGRs), which are now believed to probably be a separate class of galactic sources (although the classical GRB behaviour reported by Fenimore, Klebesadel and Laros 1996 of the 5th March 1979 outburst

at early times can support proponents of GRB-SGR associations), there have been no attenuation-type turnovers or cutoffs observed in a GRB spectrum. High energy gamma-ray emission therefore may be common in bursts, and the EGRET detection rate is consistent (Dingus 1995, though this inference is subject to poor statistics) with all bursts emitting above about 30 MeV. Observed GRB spectra are therefore in direct conflict with predicted pair production cutoffs for isotropic emission.

An obvious solution (e.g. Krolik and Pier 1991, Fenimore, Epstein and Ho 1992) is to allow some anisotropy of the emission, so that the interaction angles θ_{ti} of the photons are restricted. The threshold for pair production, $\varepsilon_t = 2/[\varepsilon_i(1-\cos\theta_{ti})]$ where ε_t and ε_i are the energies of a test photon and an interacting photon in units of $m_e c^2$, could therefore be increased above the maximum observed energy. Beaming of the radiation can be achieved through relativistic motion: the radiation from a source that is isotropically emitting in the comoving frame will be beamed mostly within an angle of the order of $1/\Gamma$ in the observer's frame, where Γ is the bulk Lorentz factor. For the case of a small emitting blob moving relativistically, the pair production optical depth $\tau_{\gamma\gamma}$ is reduced by a factor $\Gamma^{-(1+2\alpha)}$ below the optical depth for isotropic radiation, where α is the photon spectral index (Krolik & Pier 1991, Baring 1993). The minimum bulk Lorentz factors required to make $\tau_{\gamma\gamma} < 1$ in the bright "superbowl" burst (GRB930131) detected by EGRET (Sommer et al. 1994) up to an energy of $\sim 1\,\mathrm{GeV}$ are $\Gamma \gtrsim 10^3$ at a distance of 1 Gpc and $\Gamma \gtrsim 10$ at 30 kpc (Harding 1994, Harding & Baring 1994). In this case of relativistic beaming within angle $1/\Gamma$, the required luminosity L at the source is smaller because the observed flux, $\phi \sim \Gamma^2 L/4\pi d^2$, is enhanced by a solid angle factor Γ^2 (Krolik & Pier 1991). However, the number of sources must be a factor Γ^2 higher in order to account for the observed number of GRBs. In the case of cosmological GRBs, this factor could be as high as 10^6 for the above limits on Γ. This is unacceptably large for many of the proposed models, including neutron star–neutron star or neutron star–black hole mergers (Paczyǹski 1986; Eichler et al. 1989; Narayan, Piran and Shemi 1991; Mészáros & Rees 1992), failed Type 1b supernovae (Woosley 1993) and rapid spin-down of high-field millisecond pulsars (Usov 1992), and hence defines the so-called "number problem" for beamed cosmological bursts.

Source geometries with beaming angles larger than $1/\Gamma$ could ease this problem if the high energy photons were able to escape. In fact, the radiation from GRB sources in the Galactic halo or at cosmological distances is expected to involve a wind or fireball expanding relativistically (Paczynski 1986, Goodman 1986, Piran and Shemi 1993). Fenimore, Epstein & Ho (1993) have shown that a relativistically-expanding, thin spherical shell will allow escape of high energy gamma-rays, because a test photon on the surface of the shell will not be able to interact with all other emitted photons due to causality limits. This arises as a consequence of the transient nature of the emission, since then only photons emitted within a "look-back" surface around the test photon will interact to contribute to the pair production optical depth. The Fenimore, Epstein & Ho (1993) calculation was limited to the case of an infinitely thin shell.

In this study, we have extended the calculation of the pair production optical depth in GRB sources to the full range of source geometries: opening angles from $1/\Gamma$ to a spherical expansion,

and shells of arbitrary thickness. The optical depth for test photons emitted within the expanding shell will be limited to interaction with other photons within a "look-back" volume. We present analytic development and simplification of the pair production optical depth, make detailed numerical calculations, and derive analytic expressions in various limits. The intent is to provide a model-independent evaluation of the pair production opacity of a relativistically expanding, transient gamma-ray source whose emitted spectrum extends above observed energies. Using our results, we derive estimates for the minimum bulk Lorentz factors required for source transparency in those GRBs detected by EGRET at high energies. These limits are largely insensitive to the source opening angle provided that it exceeds $1/\Gamma$. This reflects the strong impact of causality in determining the optical depth, and clearly renders the number problem for cosmological source models a non-issue: the total negation of this number problem for a wide range of expansion geometries is a principal conclusion of this paper. A detailed description of the source geometry and the derivation of an analytic form for the pair production optical depth (and associated limiting cases) for infinite power-law source spectra are presented in Section 2; there the general quintuple integral expression for $\tau_{\gamma\gamma}$ [see Eq. (20)] is expediently reduced to a comparatively simple single integration in Eq. (37), a principal result of this research, rendering our developments quite amenable to various observational and theoretical applications. Section 3 is devoted to the application of these results to EGRET bursts and the estimation of minimum bulk Lorentz factors in these sources, including a discussion of the behaviour of our results in relevant parameter spaces and various issues pertaining to our calculations. Readers more interested in the applications and implications of our calculations than in the detailed derivations presented in Section 2 should note that Eq. (37) is the final form for the pair production optical depth, which should be used in conjunction with the normalization specified via the flux in Eq. (18).

2. THE PAIR PRODUCTION OPTICAL DEPTH

The generic picture of a gamma-ray burst that is considered here assumes the photon source (i.e. region of emission) to be expanding with constant and homogeneous bulk Lorentz factor Γ, with opening angle $2\Theta_{\rm B}$ about some axis and thickness ΔR (constant throughout) in the observer's frame, and with the initial condition (at time $t = 0$) that the source's inner radius is R_0. The expansion therefore traces a conical volume and can assume a variety of geometries such as solid cones, solid spheres or spherical shells, at any given time, depending on the values of the input parameters $\Theta_{\rm B}$ and $\Delta R/R_0$. The constancy of Γ in time is a convenient assumption that is not strictly valid during early epochs of the expansion if $\Delta R/R_0$ is not much less than unity: when $\Delta R/R_0 \gtrsim 1$, the expansion initially resembles a quasi-isotropic and almost stationary radiation gas in the observer's frame. The adiabatic redistribution of momenta that naturally occurs in expanding (and "inert") photon gases is therefore neglected. We also opt to ignore the consideration of possible dynamic acceleration or deceleration of the underlying plasma, since such dynamics are quite model-dependent.

Suppose that a test (i.e. potentially observable) photon, with energy $\varepsilon_t m_e c^2$, is emitted at time $t = 0$ from the inner radius R_0 of the shell and moves through the source to eventually escape and reach the observer. We opt for test photons originating at the back of the expansion throughout this paper; starting these photons closer to the outer surface will reduce the optical depth they encounter by a factor of order unity, so that the results we obtain will be qualitatively representative of general initial positions for test photons within the source. If the angle cosine between the test photon's momentum and position vectors is μ_t, then the radial distance r_t of the test photon from the center of the expansion, at any time t, is

$$r_t \;=\; R_0 + \mu_t c t \quad . \tag{1}$$

The overall geometry of this source expansion is depicted in Fig. 1a and is discussed in more detail below. Radial propagation of the test photon along the axis of the expansion corresponds to $\mu_t = 1$. An important assumption about the expansion that is made in this paper is that no photons are present prior to time $t = 0$. This "switch-on" stipulation restricts the photon population that can causally interact with the test photon at early times, and indeed mimics burst temporal behaviour; it is anticipated that the details of the switch-on will have only a quantitative rather than a qualitative influence on the results presented. The objective of this section is to derive an analytic expression for the pair production optical depth for this expanding source geometry. Consideration of the influence of the plasma that is present in the emission region on the photons it generates will be omitted from this analysis.

The optical depth for two-photon pair production $\gamma\gamma \rightarrow e^+e^-$ can be obtained from well-known expressions for the reaction rate $R_{\gamma\gamma}$ for interactions of photons in a single population (e.g. see Eq. (27) of Weaver 1976, or Eq. (7) of Stepney and Guilbert 1983). In the case where one photon is a test photon of dimensionless energy ε_t, the optical depth, differential in the distance r_t that the test photon travels, is (e.g. see Eq. (7) of Gould and Schreder 1967)

$$\frac{d\tau_{\gamma\gamma}(\varepsilon_t)}{dr_t} \;=\; \frac{1}{2}\int \sigma_{\gamma\gamma}(\chi)\,(1-\mu_{ti})\,n(\varepsilon_i,\,\mu_{ti};\,r_t)\,d\varepsilon_i\,d\mu_{ti} \quad . \tag{2}$$

Here subscripts i denote quantities of the photon that interacts with the test photon, $\chi = \sqrt{\varepsilon_t\varepsilon_i(1-\mu_{ti})/2}$ is the center-of-momentum (CM) frame energy scaled by $m_e c^2$, and

$$\sigma_{\gamma\gamma}(\chi) \;=\; \frac{\pi r_e^2}{\chi^6}\left\{(2\chi^4+2\chi^2-1)\,\log_e\Big[\chi+\sqrt{\chi^2-1}\,\Big]-\chi(1+\chi^2)\sqrt{\chi^2-1}\,\right\} \quad . \tag{3}$$

is the Lorentz-invariant pair production cross-section (e.g. see Eq. (13–40) of Jauch and Rohrlich, 1980), where $r_e = e^2/m_e c^2$ is the classical electron radius. Hereafter, all photon energies will be assumed to be dimensionless, being scaled by $m_e c^2$. Also, $\mu_{ti} = \cos\theta_{ti}$ is the angle between the momentum vectors of the test and interacting photons, and $n(\varepsilon_i,\,\mu_{ti};\,r_t)$ is the source photon density distribution at the position of the test photon. The factor of 1/2 in Eq. (2) is the standard correction for double-counting in interactions of identical particles; it is omitted in the calculations of Epstein (1985; see his Eq. 2.8) and Zdziarski (1984), who treat the test photons as a separate population from the interacting photons.

It is instructive to identify the typical energy ε_i of photons that interact with test photons at ε_t, specifically for an expansion of bulk Lorentz factor Γ that spawns power-law photon spectra, the conditions pertaining to the analysis of this paper. For such test photon energies, the minimum possible energy of the interacting photons, defined by the pair production threshold, is $\sim \Gamma/\varepsilon_t$ in the rest frame of the expansion, and of the order of Γ^2/ε_t in the stationary observer's reference frame. The pair production cross-section in Eq. (3) peaks not far above threshold, and since the optical depth is a convolution of this cross-section and the spectrum, which is a strongly decreasing function of energy, it is clear that the typical energy of an interacting photon is usually never far above threshold, i.e. around Γ^2/ε_t in the observer's frame. This result holds regardless of the source photon density provided phase space near threshold is accessible, which always is the case for infinite power-law spectra.

2.1. Source Geometry

Before developing the calculation of the pair production optical depth it is both necessary and elucidating to elaborate the details of the expansion geometry and define useful spatial variables. The general picture of the expansion at any instant is given in Fig. 1a; the definitions of the test and interacting photons' spatial and angular variables are depicted in Fig. 1b and are now enunciated. The radius of the test photon at any time is given by Eq. (1) and the angle between the radius vector (OT in Fig. 1b) to the test photon and the cone axis (OZ in Fig. 1b), which bisects $2\Theta_{\rm B}$, is defined as Θ_t ($\leq \Theta_{\rm B}$). If the expansion has an inner radius R at time t and has a thickness ΔR that is constant in time, then the test photon remains within the expanding volume only when

$$R \;=\; R_0 + \beta ct \;\leq\; r_t \;\leq\; R_0 + \Delta R + \beta ct \quad , \tag{4}$$

where $\beta = \sqrt{1-1/\Gamma^2}$ is the bulk velocity of the expansion (in units of c). In general, the angle between the test photon's position and momentum vectors is $\theta_t = \arccos\mu_t$; however, unless otherwise stated, in subsection 2.1 and subsequent portions of the paper, θ_t will be assumed to be zero so that $r_t = R_0 + ct$; this will be a specialization to the most salient case of radial propagation of test photons. Eq. (4) leads to the determination of the time t_e the test photon takes to escape the expanding plasma:

$$t_e \;=\; \frac{\Delta R}{c(1-\beta)} \quad . \tag{5}$$

Of course, calculation of the pair production optical depth will involve an integration over times $0 \leq t < \infty$, including when the test photon has escaped the expanding plasma.

The test photon interacts with photons at positions within some causally-connected look-back volume. Detailed considerations of such look-back regions for relativistic expansions are presented in Rees (1966), Fenimore, Epstein and Ho (1993). Suppose that a typical interacting photon is located at a radius r_i with the angle between its position vector (OI) and the expansion axis (OZ) being Θ_i (see Fig. 1b). Such an interacting photon was emitted at time t_i ($0 < t_i < t$) and at

a distance $r_{ti} = c(t - t_i)$ from the test photon. Let Θ_{ti} be the angle between the radius vectors (OT and OI in Fig. 1b) of the test and interacting photons. Further let the angle between the momentum vectors of the test and interacting photons be θ_{ti}. If the line (TI in Fig. 1b) between the positions of the test and interacting photons makes an angle θ_i with the radius vector of the interacting photon, then simple geometrical analysis gives

$$\begin{aligned} r_{ti}^2 &= r_t^2 + r_i^2 - 2r_t r_i \cos\Theta_{ti} \quad , \\ r_i^2 &= r_t^2 + r_{ti}^2 - 2r_t r_{ti} \cos(\theta_i - \Theta_{ti}) \quad , \\ r_t^2 &= r_i^2 + r_{ti}^2 + 2r_i r_{ti} \cos\theta_i \quad . \end{aligned} \tag{6}$$

These relationships will be used to develop the integrations in the expression for the optical depth that is derived in the following subsection. In general, if ϕ is the angle between the planes defined by the test photon momentum and position vectors and the momentum vectors of the test and interacting photons, then spherical trigonometry yields

$$\cos(\theta_i - \Theta_{ti}) \;=\; \cos\theta_t \cos\theta_{ti} - \sin\theta_t \sin\theta_{ti} \cos\phi \quad . \tag{7}$$

However, when specializing to the case of radial propagation of test photons, the photon momenta lie in the OTI plane so that $\phi = \pi$ and $\theta_i = \theta_{ti} + \Theta_{ti}$; this simplification will be used in subsequent sections.

The geometry of the source defined above, restricts the values of the variables r_{ti} and θ_{ti} that prescribe the position of the interacting photons. These restrictions arise because the interacting photons can only be emitted from the portion of the region that the expanding plasma occupied at the time of emission that is causally connected to the test photon. In the radial direction, the volume that the emission region occupies at time $t = t_i$ is specified simply by

$$R_i \;\le\; r_i \;\le\; R_i + \Delta R \quad , \quad R_i \;=\; R_0 + \beta c t_i \quad , \tag{8}$$

where the relation $r_{ti} = c(t - t_i)$ implies that $R_i = (1-\beta)R_0 + \beta(r_t - r_{ti})$. With the aid of Eq. (7), this radial constraint becomes

$$\frac{r_t^2 + r_{ti}^2 - (R_i + \Delta R)^2}{2r_t r_{ti}} \;\le\; \cos(\theta_i - \Theta_{ti}) \;\le\; \frac{r_t^2 + r_{ti}^2 - R_i^2}{2r_t r_{ti}} \quad , \tag{9}$$

which, for the case of radially-propagating test photons (i.e. when $\theta_i - \Theta_{ti} = \theta_{ti}$), is a compact representation of the limits to the μ_{ti} integration in Eq. (2). The values of r_{ti} that are achievable are further constrained by the causality condition

$$0 \;\le\; r_{ti} \;\le\; ct = \frac{r_t - R_0}{\mu_t} \quad . \tag{10}$$

In fact, this restriction automatically guarantees that $(r_t^2 + r_{ti}^2 - R_i^2)/(2r_t r_{ti}) \ge 1$ and therefore that the right hand inequality of Eq. (9) is always satisfied. Physically this occurs because interacting photons emitted at the rear of the expanding volume can never catch the test photon.

The constraints that the emission volume places on angles are simply enunciated. The requirement that the interacting photon be within the expanding shell imposes no restriction on the radial variables, but does constrain Θ_i according to

$$0 \;\leq\; \Theta_i \;\leq\; \Theta_{\rm B} \quad . \tag{11}$$

A similar condition limits the values of Θ_t at $t = 0$. Eq. (11) restricts the allowable azimuthal angles of the interacting photon for off-axis propagation of test photons; discussion of this restriction is deferred to section 2.2.2 below, specifically Eq. (25). In addition, the range of Θ_{ti} is clearly bounded by the expansion geometry. Inspection of Fig. 1b reveals that the maximum possible value of Θ_{ti} is $\Theta_{\rm B} + \Theta_t$; with the aid of Eq. (7) this becomes the global Θ_{ti} constraint

$$\cos\Theta_{ti} \;=\; \frac{1 - \rho\mu_{ti}}{\sqrt{1 - 2\rho\mu_{ti} + \rho^2}} \;\geq\; \zeta \;\equiv\; \cos\Big(\min\{\pi,\; \Theta_{\rm B} + \Theta_t\}\Big) \quad , \tag{12}$$

where $\rho = r_{ti}/r_t$ is a scaling of r_{ti} that proves convenient in the algebraic manipulations of this paper (see immediately below). This can be inverted to find the ranges of acceptable values of $\mu_{ti} = \cos\theta_{ti}$, as is outlined below in Eq. (31). This concludes the presentation of the general forms for the constraints the source geometry places on the spatial variables defined; specific developments in subsequent sections are made according to algebraic need.

It shall prove convenient to define three dimensionless variables that will facilitate the algebraic developments of the optical depth that are performed in this paper:

$$\rho \;=\; \frac{r_{ti}}{r_t} \quad , \quad \psi \;=\; \frac{r_t}{R_0} \quad , \quad s \;=\; \frac{1}{1-\rho}\,\sqrt{1 - 2\rho\mu_{ti} + \rho^2} \quad . \tag{13}$$

The first two of these are scaling transformations that define the coupling of length scales in the expansion; they are used to reduce the number of integrations in the optical depth over spatial variables by one [see Eq. (28)]. Note that the causality condition in Eq. (10) yields $0 \leq \rho \leq 1$ for $\mu_t = 1$. The definition of s is effectively an alternative to the angular variable μ_{ti} that proves convenient in reducing the integration of interacting photon angles analytically (see Section 2.3). These three variables will be referred to extensively in subsequent equations.

Hereafter, this paper addresses the special case of radial propagation of test photons along the axis of the expansion, so that $\mu_t = \cos\theta_t = 1$ and $\Theta_t = 0$. While this choice is motivated by the simplifications it introduces to the analysis, it is concordant with the goal of obtaining representative estimates of source bulk Lorentz factors that are consistent with GRB observations. Relativistically expanding sources contribute most of their observable emission along the direction of motion, corresponding to radial and on-axis propagation of the test photons. Off-axis (i.e. non-radial) emission will mostly be outside the peak of beamed radiation, and therefore form only a minor part of the observable flux of gamma-rays. Hence we expect that photons produced somewhat off-axis will contribute minimally to the observed flux, and therefore be largely irrelevant to the determination of minimum bulk Lorentz factors. A brief discussion of this specialization, in the

light of the results obtained, is presented in Section 4. Note that while "limb" photons move on average at large angles to the beamed photon population in their locale, the phase space that connects them causally to the remaining photon population is small; it is not clear whether or not limb photons will have enhanced pair production optical depths relative to line-of-sight radiation.

2.2. Analytic Reduction of The Optical Depth

The differential optical depth in Eq. (2) can be developed once the photon distribution function $n(\varepsilon_i,\, \mu_{ti};\, r_t)$ is known, and eventually an integration over r_t will be performed to obtain the total optical depth $\tau_{\gamma\gamma}(\varepsilon_t)$. The form that $n(\varepsilon_i,\, \mu_{ti};\, r_t)$ takes depends on basic assumptions about the expanding photon gas. In this paper, the *rate of photon emission* is taken to be constant in time and space after time $t = 0$ (following, for example, Fenimore et al. 1993, but in contrast to the uniform density choice made by Harding and Baring 1994), but is zero for $t < 0$, and is isotropic only in the comoving frame of the expansion. This simplifying assumption is made for its convenience; it is unrealistic since it may be acausal for some initial conditions (e.g. the instantaneous "switch-on" over a finite volume). Observed temporal behaviour in individual sources is somewhat chaotic (e.g. see the BATSE 1B catalogue, Fishman et al. 1994), so the assumption of constant emissivity is not truly accurate, depending on the timescale of specific consideration. However, in conjunction with the source geometry prescribed here, a constant emissivity may be able to approximately produce global properties of bursts, such as longer average decay timescales than rise times (Nemiroff et al., 1994; Norris, et al. 1994; Mitrofanov 1995). Our assumption of a temporally-invariant emissivity after switch-on is an appropriate approximation for the objectives of this paper, since only estimates of the bulk relativistic motion in gamma-ray bursts are at present obtainable as the origin of bursts is still uncertain. Note that the rate of emission might be expected to decline in time due to expansion effects such as adiabatic cooling and a decrease in plasma density.

An immediate consequence of this approximation is that the photon distribution in the comoving frame of the expansion is anisotropic even for isotropic photon emission, due to radiative transfer effects in finite source volumes. This assumption is clearly different from the premise of Gould and Schreder (1967), from which the bulk motion analyses of Krolik and Pier (1991) and Baring (1993) are derived, who all effectively assumed that the photon *distribution* is everywhere and at all times isotropic (Krolik and Pier 1991 actually invoked the equivalent assumption of isotropy of the photon intensity in the comoving frame). Isotropy of the photon distribution is an even more elementary approximation: it is perhaps less realistic than the assumption of isotropic emission rate that is made here, given that isotropic radiation fields are usually best generated in optically (Thomson) thick media, contrary to the basis of these pair-production calculations. Isotropic emissivities require only that the supporting particle population is isotropic, and that there is no other preferred direction in the emission region, such as that imposed by the presence of a magnetic field.

2.2.1. Photon density and the observed flux

For a constant rate of photon emission, the photon distribution at any point is simply obtained by adapting standard radiative transfer results (e.g. see Rybicki and Lightman, 1979) to the consideration of photon densities. The conservation of photon numbers and volume elements along light rays in optically thin environments automatically yields conservation of the number density, from which the transfer equation yields

$$n(\varepsilon_i,\, \mu_{ti};\, r_t) \;=\; \frac{1}{c}\int \dot{n}(\varepsilon_i,\, \mu_i;\, r_i)\, dr_{ti}\, \frac{d\phi_{ti}}{2\pi} \quad . \tag{14}$$

Here r_{ti} traces out the photon path through the look-back volume and $\dot{n}(\varepsilon_i,\, \mu_i;\, r_i)/2\pi$ is the rate of photon emission in the observer's frame, per unit solid angle, at the position of the interacting photon (the point labelled I in Fig. 1b). The arguments of the emission rate in the integrand are implicitly functions of the spatial variables relating to the test photon position, i.e. $\mu_i = \cos\theta_i = \mu_i(r_t,\, t_{ti},\, \mu_{ti})$ and $r_i = r_i(r_t,\, t_{ti},\, \mu_{ti})$ are defined by Eq. (7), and determined by the geometry in Fig. 1b. Here $\mu_{ti} = \cos\theta_{ti}$. Throughout the following analysis, it is assumed that $\theta_t = 0$. The angular dependence of the distribution and emission rate has been retained because of the highly anisotropic conditions encountered in this calculation. The azimuthal angle ϕ_{ti} is defined to be the angle between the OZT and OZI planes in Fig. 1b. Since the emission rate is independent of position within the expanding volume, no azimuthal dependence appears in the arguments of $\dot{n}(\varepsilon_i,\, \mu_i;\, r_i)$. Note that Harding and Baring (1994) combine Eqs. (2) and (14) into a single expression for the optical depth in their Eq. 2; their result is mildly erroneous, being a factor of $2/\pi$ too small.

If the source generates isotropic radiation in the comoving frame of the expansion with a power-law emission spectrum $\dot{n}_c(\varepsilon_c,\, \mu_c) \propto \varepsilon_c^{-\alpha}$, where ε_c and μ_c are the photon energy and emission angle in the comoving frame, then it follows that the photon emission rate in the observer's frame takes the form

$$\dot{n}(\varepsilon,\, \mu,\, r) \;=\; \dot{\mathcal{N}}\, \varepsilon^{-\alpha}\, (1-\beta\mu)^{-(1+\alpha)} \quad , \quad \varepsilon_- \,\le\, \varepsilon \,\le\, \varepsilon_+ \quad , \tag{15}$$

where $\varepsilon_\pm$ define the bounds to the observed source spectrum. This form is derived from the Lorentz transformation relationships $\varepsilon_c = \Gamma\varepsilon(1-\beta\mu)$ and $\mu_c = (\mu-\beta)/(1-\beta\mu)$ and their associated Jacobian $d\varepsilon_c\, d\mu_c/d\varepsilon\, d\mu = [\Gamma(1-\beta\mu)]^{-1}$, given that the total photon number $\dot{n}(\varepsilon,\, \mu,\, r) d\varepsilon d\mu\, dV\, dt$ is a Lorentz invariant. Note that in Eq. (15), a factor of $1/\Gamma$ has been absorbed in the definition of $\dot{\mathcal{N}}$.

The value of the coefficient $\dot{\mathcal{N}}$ in Eq. (15) can be determined by computing the photon flux $\mathcal{F}$ at large distances from the source and equating the result to the observed flux in individual GRBs. Specifically, the flux at test photon energy $\varepsilon_t = 1$ (i.e. 511 keV) is

$$\mathcal{F} \;=\; c\int d\mu_{ti}\, \mu_{ti}\, n(\varepsilon_t{=}1,\, \mu_{ti},\, r_t) \;=\; \dot{\mathcal{N}}\int \frac{\mu_{ti}}{(1-\beta\mu_i)^{\alpha+1}}\, d\mu_{ti}\, dr_{ti} \quad , \tag{16}$$

after integrating Eq. (14) over azimuthal angles. The units of $\mathcal{F}$ are photons per square centimetre per second. For the moment assume that there are no angular restrictions to the phase space, i.e.

$\Theta_{\rm B} = \pi/2$. Further, note that in this integral the test photon acts purely as a position marker and can be taken to be on-axis without loss of generality, i.e. $\Theta_t = 0$. The angle cosine μ_i in the distribution is given by Eq. (23) below, and the limits on the integrals are defined by the radial and causality constraints in Eqs. (9) and (10). At large distances from the source, these restrictions imply that $r_{ti}/r_t \approx 1$ and $\mu_{ti} \approx 1$, as is obvious from the description of the geometry in Fig. 1a. In fact, defining $\psi = r_t/R_0$, then Eqs. (9) and (10) can be expressed as $\psi_- \le \psi \le \psi_+$, where $\psi_\pm$ are given in Eq. (29). The evaluation of the integrals in Eq. (16) can be facilitated by changing variables thus: the μ_{ti} integration is performed using the variable $s = \sqrt{1 - 2\rho\mu_{ti} + \rho^2}\,/(1-\rho)$ for $\rho = r_{ti}/r_t\,(\approx 1)$, and the ρ integration is calculated using the variable $t = \psi(1-\rho)$. For $\psi \gg 1$, then $\mu_i \approx 1/s$. Reversing the order of integration yields $1 \le t \le (1 - \beta + \Delta R/R_0)/(s-\beta)$ and a trivial result for the t integral, so that

$$\mathcal{F} \;=\; \frac{\dot{\mathcal{N}}}{3}\,\frac{R_0^3}{d^2}\int_1^{s_+}\frac{s^{\alpha+2}\,ds}{(s-\beta)^{\alpha+4}}\left\{\left(1-\beta+\frac{\Delta R}{R_0}\right)^3 - (s-\beta)^3\right\} \quad , \quad s_+ \;=\; 1+\frac{\Delta R}{R_0} \quad . \tag{17}$$

Here r_t is set equal to the distance d between the source and the observer, and the flux naturally obeys an inverse-square law: $\mathcal{F} \propto d^{-2}$. Note that the algebraic manipulations here closely resemble those applied to the expression for the optical depth; for this reason, detail is minimized here and is deferred to section 2.2.2 below.

In general, the result in Eq. (17) can be expressed in terms of a hypergeometric function of two variables, however it is simple to evaluate it directly by numerical integration. In the special cases where the expansion is, in the comoving frame, a thin spherical shell with $\Delta R/R_0 \ll 1-\beta$, or it is a filled shell with $\Delta R/R_0 \gg 1-\beta$, it becomes analytically tractable, giving

$$\mathcal{F} \;\approx\; \frac{\dot{\mathcal{N}}}{2}\,\frac{(\Delta R)^2}{d^2}\begin{cases}\dfrac{R_0}{(1-\beta)^{\alpha+2}} \;, & \dfrac{\Delta R}{R_0} \ll 1-\beta \quad . \\[2ex] \dfrac{2\Delta R}{3(\alpha+3)\beta}\left\{\dfrac{1}{(1-\beta)^{\alpha+3}} - 1\right\} \;, & \dfrac{\Delta R}{R_0} \gg 1-\beta \quad . \end{cases} \tag{18}$$

The quadratic dependence of $\mathcal{F}$ in ΔR when $\Delta R/R_0 \ll 1$ reflects the two dimensions of the integration in Eq. (16). At the same time, $\mathcal{F}$ is independent of R_0 when $R_0 \ll \Delta R$ since the inner radius contributes negligibly to the source volume. The value of $\dot{\mathcal{N}}$ is therefore determined by equating the flux in Eq. (17) to that observed at 511 keV for sources with unbroken power-law spectra, or by a power-law extrapolation of the high energy spectrum down to 511 keV for those sources with spectral breaks above this energy (e.g. GRB940217; see the discussion in Section 3).

The modification to the expression in Eq. (17) for the flux that is induced by reduction of $\Theta_{\rm B}$ below $\pi/2$ is straightforward. The considerations of angular constraints in subsection 2.1 lead to the simple expression for the restriction of the $(\,\mu_{ti}\,,\;\rho\,)$ phase space in Eq. (12). Since the flux is observed at infinity, $\mu_{ti} \approx 1$ and we take $\Theta_t = 0$ for the flux calculation. Then Eq. (12) immediately implies that $s \le 1/\zeta$, for ζ defined just below in Eq. (19), and it quickly follows that

sub-spherical expansions generate a flux given by Eq. (17) but with

$$s_+ \;=\; \min\Bigl\{1+\frac{\Delta R}{R_0}\,,\;\frac{1}{\zeta}\Bigr\} \quad , \quad \zeta \;=\; \cos\Bigl(\min\{\pi,\;\Theta_{\rm B}\}\Bigr) \tag{19}$$

substituted as the upper limit to the integral. Clearly then, the angular restrictions play no role in determining the flux until the solid angle $[\,2\pi(1-\cos\Theta_{\rm B})\,]$ of the expansion becomes comparable to the fractional shell thickness $\Delta R/R_0$.

2.2.2. Optical depth for radial propagation of test photons

The differential optical depth in Eq. (2) can now be expressed in more explicit form using Eq. (14) and the form of the photon emission rate in Eq. (15), evaluated at the position of the interacting photon:

$$\frac{d\tau_{\gamma\gamma}(\varepsilon_t)}{dr_t} \;=\; \frac{\dot{\mathcal{N}}}{4\pi c}\int \sigma_{\gamma\gamma}(\chi)\,\varepsilon_i^{-\alpha}\,\frac{1-\mu_{ti}}{(1-\beta\mu_i)^{\alpha+1}}\,d\varepsilon_i\,d\mu_{ti}\,dr_{ti}\,d\phi_{ti} \quad . \tag{20}$$

Here $\dot{\mathcal{N}}$ has been removed from the integration because it is assumed to depend only on $\Theta_{\rm B}$ and be independent of the position within the source. Hereafter it will be assumed that the emission spectrum in Eq. (15) has a large or infinite range ($\varepsilon_+ \gg \varepsilon_-$), for which it is possible evaluate the ε_i integration separately, and analytically. Specifically, it is permissible to change variables in Eq. (20) to the CM frame energy variable $\chi = \sqrt{\varepsilon_t\varepsilon_i(1-\mu_{ti})/2}$ via $4\chi d\chi = \varepsilon_t(1-\mu_{ti})d\varepsilon_i$, following the procedure of Gould and Schreder (1967; see also Baring, 1993), and perform the integration of the cross-section separately. Consequently, the differential optical depth assumes the form

$$\frac{d\tau_{\gamma\gamma}(\varepsilon_t)}{dr_t} \;=\; \dot{\mathcal{N}}\,\frac{\sigma_{\rm T}}{\pi c}\,\varepsilon_t^{\alpha-1}\,\frac{\mathcal{H}(\alpha)}{2^{\alpha+2}}\int \frac{(1-\mu_{ti})^{\alpha}}{(1-\beta\mu_i)^{\alpha+1}}\,d\mu_{ti}\,dr_{ti}\,d\phi_{ti} \quad , \tag{21}$$

where the integration of the cross-section over χ is

$$\mathcal{H}(\alpha) \;=\; \frac{4}{\sigma_{\rm T}}\int_1^\infty \chi^{1-2\alpha}\sigma_{\gamma\gamma}(\chi)\,d\chi \;\approx\; \frac{7}{6\alpha^{5/3}} \quad . \tag{22}$$

The approximation in Eq. (22) was obtained (see Baring, 1993) from Eq. B6 of Svensson (1987), who also gave the exact analytic expression for the integral; it is accurate to better than 1% for $1<\alpha<7$. The angle cosine $\mu_i = \cos\theta_i$ of the interacting photon that appears in Eq. (21) can be determined explicitly from the geometry in Fig. 1b using Eq. (7); eliminating the variables r_i and Θ_{ti} gives (for $\theta_t = 0$)

$$\mu_i \;=\; \frac{\mu_{ti}-\rho}{\sqrt{1-2\rho\mu_{ti}+\rho^2}} \quad . \tag{23}$$

The scaling variable $\rho = r_{ti}/r_t$ (<1 for $\mu_t = 1$) will be of use in the development of the optical depth integration.

In applications where the emission spectrum is of finite energy range, the modification for performing the ε_i integration has been developed by Gould and Schreder (1967) and Krolik and Pier (1991). Low energy spectral turnovers or cutoffs are unlikely to be influential in pair production continuum attenuation calculations applied to gamma-ray bursts that have bulk motions with large Lorentz factors Γ and maximum energies under 100 MeV (Baring, 1994). While turnovers are observed as photon energies drop into the BATSE range, sharp cutoffs can presumably be only in the soft X-ray range where photons interact with gamma-rays of energy much more than 1 GeV to produce pairs. Therefore any suppression of $\gamma\gamma \to e^+e^-$ continuum attenuation that is introduced by a low-energy cutoff is unlikely to be observed by EGRET. However, for observations in the super-GeV range, spectral structure in the BATSE range becomes quite relevant to opacity determinations (Baring and Harding 1997), and is discussed briefly at the end of Section 3. Introduction of high energy cutoffs to the spectrum of interacting photons is also largely irrelevant to this investigation because the most energetic EGRET source photons predominantly interact with photons at energies considerably below the maximum detected.

The azimuthal integration in Eq. (21) can be performed after establishing the restrictions the source geometry places on ϕ_{ti}. For the interacting photon to be in the expanding "conical shell," the radial restriction in Eq. (9) is independent of ϕ_{ti}. In contrast, the angular constraint $0 \le \Theta_i \le \Theta_{\rm B}$ in Eq. (11), which is independent of time, does restrict the allowable azimuthal angles. Assuming that the plasma emits uniformly at any one time, this angular constraint results in an analytic determination of the azimuthal integration, because at a given radius each azimuthal angle within the cone of expansion *contributes equally.* Since the azimuthal angle ϕ_{ti} is defined to be the angle between the planes OZT and OTI (see Fig. 1b), then considerations of spherical trigonometry yield

$$\cos\Theta_i \;=\; \cos\Theta_t\cos\Theta_{ti} + \sin\Theta_t\sin\Theta_{ti}\cos\phi_{ti} \;\ge\; \cos\Theta_{\rm B} \tag{24}$$

when $|\Theta_t \pm \Theta_{ti}| \le \Theta_{\rm B}$. When this condition is not satisfied, the interacting photon is always within the cone defined by the expansion and all values $0 \le \phi_{ti} \le 2\pi$ are permitted. It follows that the ϕ_{ti} integration has limits defined by $|\cos\phi_{ti}| \le \eta$, where

$$\eta \;=\; \begin{cases} \dfrac{\cos\Theta_{\rm B} - \cos\Theta_t\cos\Theta_{ti}}{\sin\Theta_t\sin\Theta_{ti}} \;\;, & \Theta_{\rm B} - \Theta_t \le \Theta_{ti} \le \Theta_{\rm B} + \Theta_t \;\;, \\ -1 \;\;, & 0 \le \Theta_{ti} \le \Theta_{\rm B} - \Theta_t \;\;. \end{cases} \tag{25}$$

The restriction $\Theta_{ti} > \Theta_{\rm B} - \Theta_t$ is necessary to achieve $\eta > -1$, and as $\Theta_{ti} \to \Theta_{\rm B} + \Theta_t$ then $\eta \to 1$ and the permitted ϕ_{ti} phase space shrinks to zero. When $\Theta_t \to 0$, (i.e. the test photon is on the axis of the expansion), $\eta \to -1$ for all permissible Θ_{ti}. This simple special case will be assumed throughout subsequent sections of the paper. The ϕ_{ti} integration in Eq. (21) is then trivially evaluated to give $2\arccos\eta$. Equation (21) can then be integrated over the test photon position r_t to give the total optical depth:

$$\tau_{\gamma\gamma}(\varepsilon_t) \;=\; \dot{\mathcal{N}}\,\frac{\sigma_{\rm T}}{\pi c}\,\varepsilon_t^{\alpha-1}\,\frac{\mathcal{H}(\alpha)}{2^{\alpha+1}}\int \arccos\eta\,\frac{(1-\mu_{ti})^{\alpha}}{(1-\beta\mu_i)^{\alpha+1}}\,d\mu_{ti}\,dr_{ti}\,dr_t \quad , \tag{26}$$

and the value for η when $|\Theta_t \pm \Theta_{ti}| \leq \Theta_{\rm B}$ becomes (for $\theta_t = 0$)

$$\eta \;=\; \frac{\cos\Theta_{\rm B}\sqrt{1-2\rho\mu_{ti}+\rho^2} \;-\cos\Theta_t(1-\rho\mu_{ti})}{\rho\sin\Theta_t\sqrt{1-\mu_{ti}^2}} \quad , \tag{27}$$

where the substitution for Θ_{ti} has been effected using Eq. (7), the variable ρ is defined in Eq. (13), and the sine rule applied to triangle OTI in Fig. 1b.

For the moment, consider 4π steradian expansions, where $\Theta_{\rm B} = \pi$ and angular restrictions to the interaction phase space do not enter the analysis. Evaluation of the triple integral in Eq. (26) can be facilitated by changing variables via the scaling transformations defined in Eq. (13), so that μ_i and η are rendered independent of r_t (see Eqs. (23) and (27)). A complete set of dimensionless variables has therefore been chosen and reversing the order of integration so that the ψ integration is performed first yields an analytic reduction of the optical depth to a double integral:

$$\tau_{\gamma\gamma}(\varepsilon_t) \;=\; \dot{\mathcal{N}}\,\frac{\sigma_{\rm T}}{\pi c}\,R_0^2\,\varepsilon_t^{\alpha-1}\,\frac{\mathcal{H}(\alpha)}{2^{\alpha+2}}\int_0^1 d\rho\int_{\mu_{\rm MIN}}^1 d\mu_{ti}\;(\psi_+^2-\psi_-^2)\;\arccos\eta\,\frac{(1-\mu_{ti})^\alpha}{(1-\beta\mu_i)^{\alpha+1}} \quad . \tag{28}$$

The value of $\mu_{\rm MIN}$ is given in Eq. (30). Here $\psi_\pm$ are the limits of the ψ integration ($\psi_- \leq \psi \leq \psi_+$), and are determined from the radial constraint in Eq. (9) and the causality condition in Eq. (10):

$$\psi_- \;=\; \frac{1}{1-\rho} \quad , \quad \psi_+ \;=\; \frac{1-\beta+\Delta R/R_0}{\sqrt{1-2\rho\mu_{ti}+\rho^2}-\beta(1-\rho)} \quad , \tag{29}$$

where $0 \leq \rho \leq 1$ defines a "look-back" volume. If the expansion is at least fully hemispherical ($\Omega \geq 2\pi$), then $\eta = -1$, and the μ_{ti} integration is over a range determined by the condition $\psi_+ \geq \psi_-$. It follows from Eq. (29) that the range of μ_{ti} permitted in Eq. (28) is $\mu_{\rm MIN} \leq \mu_{ti} \leq 1$, where, for *any* $\beta < 1$,

$$\mu_{\rm MIN} \;=\; \begin{cases} \dfrac{1}{2\rho}\Big\{1+\rho^2-(1-\rho)^2\Big(1+\dfrac{\Delta R}{R_0}\Big)^2\Big\} \;, & \dfrac{\Delta R}{2R_0+\Delta R} \;<\; \rho \;\leq\; 1 \;, \\ -1 \;, & \text{otherwise.} \end{cases} \tag{30}$$

Clearly $\mu_{\rm MIN} \leq 1$ is always true. This restriction indicates that the look-back volume is not spherical because of the presence of edges to the expansion in the radial direction. The form of the pair production optical depth in Eq. (28) is not generally reducible to a simpler form, and is ready for numerical evaluation in cases where $\Theta_{\rm B} \geq \pi/2$. However, analytic development is possible in the special case of propagation of test photons along the axis of the expansion (i.e. $\Theta_t = 0$), which will be treated in the next subsection.

Consider now the additional restrictions on the integration phase space due to a reduction in the expansion opening angle $\Theta_{\rm B}$. The way the expansion has been defined automatically precludes any necessity to treat cases where $\Theta_{\rm B} > \pi/2$, since they reduce to the $\Theta_{\rm B} = \pi/2$ case. This arises because switching on the expansion at $t = 0$ implies that interacting photons from the back hemisphere $\Theta_i > \pi/2$ (for $\Theta_t = 0$) can never reach the test photon originating in the forward

hemisphere, and therefore cannot contribute to the optical depth. This switch-on stipulation is a reasonable approximation to a real burst, and the contribution to the optical depth from photons originating in the back hemisphere is expected to be strongly suppressed due to the relativistic nature of the expansion. When $\Theta_{\rm B} < \pi$, both μ_{ti} and the azimuthal angle ϕ_{ti} are restricted. The constraint on Θ_{ti} in Eq. (12) can be inverted to find the ranges of acceptable values of μ_{ti} in terms of ρ, which defines how the reduction of the opening angle of the expansion restricts the (μ_{ti}, ρ) phase space:

$$-1 \;\le\; \mu_{ti} \;\le\; \mu_- \quad , \quad \mu_+ \;\le\; \mu_{ti} \;\le\; 1 \quad , \tag{31a}$$

where

$$\mu_\pm \;=\; \begin{cases} \dfrac{1}{\rho}\Big\{1-\zeta^2 \pm |\zeta|\sqrt{\rho^2+\zeta^2-1}\Big\} \;, & \rho \ge \sqrt{1-\zeta^2} \\ \sqrt{1-\zeta^2} \;, & \rho < \sqrt{1-\zeta^2} \end{cases} \tag{31b}$$

Therefore when $\rho < \sqrt{1-\zeta^2}$ all values of μ_{ti} are permitted, since then the angular boundary to the expansion lies outside the look-back volume defined by ρ. The azimuthal restrictions are reflected in the value of η in Eq. (27), and by a similar analysis, the boundary where η increases above -1 is also defined by Eq. (31), but with $\zeta \to \cos(\Theta_{\rm B} - \Theta_t)$. The ranges in Eq. (31) are, of course, subject to the $\mu_{\rm MIN} \le \mu_{ti}$ limitation that is imposed by radial considerations.

In the case where the test photon propagates radially along the axis of the expansion (i.e. $\Theta_t = 0$), which will be the focal point of all subsequent developments in this paper, the double integral expression for the optical depth in Eq. (28) can be manipulated into a form that is more convenient for numerical computation, where one integral can be expressed in terms of familiar hypergeometric functions. The analytical approach is similar to the derivation of the photon flux in Eq. (17). The μ_{ti} integration is expressed in terms of the variable s, defined in Eq. (13), and the ρ integration can be performed first using the variable $t = 1 - \rho$. This change of variables leads to the range

$$1 \;\le\; s \;\le\; 1 + \frac{\Delta R}{R_0} \quad , \tag{32}$$

for the variable s, which can be easily deduced from the requirement that $\mu_{ti} < 1$ and the condition that $\psi_+ > \psi_-$ in Eq. (29). For specific s within this range, inversion of the restriction in Eq. (30) leads to the upper bound $t_+ = 2/(1+s)$ for t, which can also be obtained equivalently from the radial constraint in Eq. (9). The lower bound to t can be derived directly from the angular constraint in Eq. (12); the result gives

$$\max\left\{0 \,, \frac{2(\zeta s - 1)}{s^2 - 1}\right\} \;=\; t_- \;\le\; t \;\le\; t_+ \;=\; \frac{2}{1+s} \quad , \tag{33}$$

where ζ is defined in Eq. (19). Since $\zeta \le 1$, it follows that $t_+ \ge t_-$ so that only one range arises for the t-integration. This simplicity does not arise if the s-integration is performed first since t_- has a maximum of $1 - \sqrt{1-\zeta^2}$ that can then yield two integration ranges for s for some t. Note that t_- exceeds zero only when $s > 1/\zeta$. Hence, the angular constraint only impacts the calculation of the optical depth when $\zeta > R_0/(R_0 + \Delta R)$, a situation identical to that arising in

the treatment of the source flux. Remembering that $\arccos\eta = \pi$ for this case of radial and axial propagation of test photons, the optical depth in Eq. (28) develops to the form

$$\begin{aligned}\tau_{\gamma\gamma}(\varepsilon_t) &= \dot{\mathcal{N}}\,\frac{\sigma_{\rm T}}{c}\,R_0^2\,\varepsilon_t^{\alpha-1}\,\frac{\mathcal{H}(\alpha)}{2^{\alpha+1}}\int_1^{1+\delta} ds\,\left[\left(\frac{1-\beta+\delta}{s-\beta}\right)^2 - 1\right] \\ &\times \quad s^{2+\alpha}\,(s^2-1)^{\alpha}\int_{t_-}^{t_+} dt\,\frac{t^{2\alpha}}{\mathcal{D}^{1+\alpha}} \quad , \quad \mathcal{D} = 2(s-\beta) + t[(1+s^2)\beta - 2s] \quad , \end{aligned} \tag{34}$$

for fractional shell thickness $\delta = \Delta R/R_0$.

The angular constraint in Eq. (12) is unimportant only when $t_- = 0$. In general, this is not so, and the t-integration in Eq. (34) can be written as the difference between integrations over the ranges $[0,\, t_+]$ and $[0,\, t_-]$. Therefore two terms appear, each of which can be manipulated in a similar fashion. Consider first the integration over $[0,\, t_-]$: the t-integration can be rewritten via the substitution $t = t_-(1-q)$, leading to the transformation

$$s^{2+\alpha}\,(s^2-1)^{\alpha}\int_0^{t_-} dt\,\frac{t^{2\alpha}}{\mathcal{D}^{1+\alpha}} = \frac{2^\alpha\sigma^{\alpha+1}}{(1+\beta)^{\alpha+1}}\,\frac{s}{s-1}\left(\frac{\zeta s-1}{s-1}\right)^{\alpha}\int_0^1 dq\,\frac{(1-q)^{2\alpha}}{(1-\sigma\lambda q)^{\alpha+1}} \quad . \tag{35}$$

Here $\lambda = \lambda(s,\,\beta)$ and $\sigma = \sigma(s,\,\beta,\,\zeta)$ are given by

$$\lambda = \frac{(1+s^2)\beta - 2s}{s(s-1)(1+\beta)} \quad , \quad \sigma = \frac{\zeta s - 1}{(s-1) - (1-\zeta)s\lambda} \quad . \tag{36}$$

It can be shown that λ is a monotonically decreasing function of s with the range $-\infty < \lambda < \beta/(1+\beta)$, and furthermore that $0 \le \sigma \le 1$. When $\zeta \to 1$ (i.e. $\Theta_{\rm B} \to 0$), then $t_- \to t_+$ and $\sigma \to 1$, so that the result for t-integration over the range $[0,\, t_+]$ is recovered. Putting the two terms together and defining the Heaviside step function $\mathcal{H}_{\rm S}(x)$ to be unity when $x > 0$ and zero otherwise, the optical depth can therefore be written in the form

$$\tau_{\gamma\gamma}(\varepsilon_t) = \dot{\mathcal{N}}\,\frac{\sigma_{\rm T}}{2c}\,R_0^2\,\varepsilon_t^{\alpha-1}\,\frac{\mathcal{H}(\alpha)}{(1+\beta)^{\alpha+1}}\int_1^{1+\delta} ds\,\frac{s}{s-1}\left[\left(\frac{1-\beta+\delta}{s-\beta}\right)^2 - 1\right]\mathcal{J}_\alpha(s;\,\beta,\,\zeta) \tag{37a}$$

for $\delta = \Delta R/R_0$, with

$$\mathcal{J}_\alpha(s;\,\beta,\,\zeta) \equiv \mathcal{G}_\alpha(\lambda) - \mathcal{H}_{\rm S}\Big(s - \frac{1}{\zeta}\Big)\left(\frac{\zeta s-1}{s-1}\right)^{\alpha}\sigma^{\alpha+1}\,\mathcal{G}_\alpha(\sigma\lambda) \tag{37b}$$

The function $\mathcal{G}_\alpha(z)$ is just the integral that appears in Eq. (35), and is expressible in terms of the standard hypergeometric function $F(\alpha,\,\beta;\,\gamma;\,z)$ using the identity 3.197.3 in Gradshteyn and Ryzhik (1980):

$$\mathcal{G}_\alpha(z) \equiv \int_0^1 dq\,\frac{(1-q)^{2\alpha}}{(1-zq)^{\alpha+1}} = \frac{1}{1+2\alpha}\,F(\alpha+1,\,1;\,2\alpha+2;\,z) \quad . \tag{38}$$

The numerical evaluation of $\mathcal{G}_\alpha$ is straightforward, and is described in the Appendix. An alternative form for the optical depth can be derived by leaving the t-integration in Eq. (34) as one integral

over the range $[t_-,\, t_+]$ and rescaling the integration variable. This second form yields Eq. (37a) but with an alternative representation of the function $\mathcal{J}_\alpha(s;\, \beta,\, \zeta)$:

$$\mathcal{J}_\alpha(s;\, \beta,\, \zeta) \;=\; \int_0^{q_+} dq\, \frac{(1-q)^{2\alpha}}{(1-\lambda q)^{\alpha+1}} \quad , \quad q_+ \;=\; \min\!\left\{1,\; \frac{s(1-\zeta)}{s-1}\right\} \quad . \tag{39}$$

While slightly less convenient than Eq. (37) for numerical evaluation of the optical depth, this second form is useful when obtaining results in the limiting case of small opening angles, treated in subsection 2.3.3 below. Computationally, if the series representation of $\mathcal{G}_\alpha$ described in the Appendix is used, Eq. (37) is a single integral that is relatively simple to evaluate. Note that the integrand does not diverge at $s = 1$ due to the behaviour of $\mathcal{G}_\alpha(\lambda)$ there (see the Appendix).

It is important to emphasize that the optical depth in Eq. (37) was obtained under the assumptions that the test photon originates at the rear of the expansion and propagates radially outward. With this specification, Eq. (37) is intended to approximate a variety of possibilities for test photon initial conditions. Non-radial test photon motion will increase the optical above that in Eq. (37), primarily because of increased angles with interacting photons, however an observer's unique perspective will strongly bias against such situations for relativistic expansions. On the other hand, test photons can plausibly originate closer to the surface of the expansion than R_0 , diminishing the optical depth accordingly. Suppose that the test photon starts at radius $R_0 + \nu\Delta R$ at time $t = 0$. Then all interacting photons inside this radius are *always* causally-disconnected from the test photon because it propagates radially. Hence the region interior to $R_0 + \nu\Delta R$ is irrelevant to the optical depth calculation, and a new initial condition can be defined, with $R_0 + \nu\Delta R$ and $R_0 + \Delta R$ denoting the relevant inner and outer radii of the expansion. The test photon is now at the rear of this section of the conical shell, and the optical depth computation can be repeated entirely with the aid of the substitution

$$R_0 \;\rightarrow\; R_0 + \nu\Delta R\,, \quad \Delta R \;\rightarrow\; (1-\nu)\Delta R \tag{40}$$

without any additional manipulation. This elementary transformation propagates all the way through the development so that the optical depth for test photons starting at arbitrary positions $R_0 + \nu\Delta R$ in the expansion is simply from Eq. (37) by the substitution $\delta \rightarrow (1-\nu)\delta/(1+\nu\delta)$, a very attractive scheme of generalization. Note that the normalizing flux in Eq. (17) is unaffected by these considerations.

This concludes the analytic development of the optical depth formula, which is ready for numerical computation and certainly is much more amenable than the quintuple integral in Eq. (20). Before presenting such computations (in subsection 2.4 below), it is instructive to examine the optical depth for some limiting cases of the source geometry.

2.3. Approximations in Limiting Cases

There are four special cases where it is both possible and useful to obtain analytic limits to the pair production optical depth: these correspond to the thin-shell limit, thick-shell or filled-sphere expansions, narrow beams, and a stationary photon gas.

2.3.1. The thin-shell limit

The expression in Eq. (37) is in suitable form for the derivation of the optical depth in certain special cases. The first of these is the limit of a thin, spherical shell for the expansion, where $\delta = \Delta R/R_0 \ll 1-\beta$ (i.e. the shell is also thin in the comoving frame of the expansion), and $\delta \ll 1-\zeta$ so that the angular constraints are immaterial. The $\mathcal{G}_\alpha(\sigma\lambda)$ term in Eq. (37) is therefore absent. As noted in the Appendix, in the $s \to 1$ limit, $(1+2\alpha)\mathcal{G}_\alpha(\lambda)$ approaches $F(\alpha+1,\,1;\,2\alpha+2;\,1)/(1-\lambda)$, which with the aid of identity 9.122 of Gradshteyn and Ryzhik (1980) leads to the limit $\mathcal{G}_\alpha(\lambda) \to 1/[\alpha(1-\lambda)] \approx (s-1)(1+\beta)/[2\alpha(1-\beta)]$. It is then elementary to derive the result $\tau_{\gamma\gamma}(\varepsilon_t) \propto \dot{\mathcal{N}}\,(\Delta R)^2$. The two powers of ΔR are due to the thin shell severely restricting the spatial extent of the r_t and r_{ti} integrations [e.g. see Eq. (20)]. Such behaviour is largely meaningless until the dependence of the formula for the flux is factored in. Remembering that in this limit, for a fixed observed flux, Eq. (18) yields $\dot{\mathcal{N}} \propto 1/(\Delta R)^2$, the optical depth is virtually independent of ΔR, as is expected. Explicitly, we obtain

$$\tau_{\gamma\gamma}(\varepsilon_t) \;\approx\; \frac{\sigma_{\rm T}}{2c}\,\frac{d^2}{R_0}\,\mathcal{F}\,\frac{\mathcal{H}(\alpha)}{\alpha}\left(\frac{1-\beta}{1+\beta}\right)^{\alpha}\varepsilon_t^{\alpha-1} \quad , \quad \frac{\Delta R}{R_0} \ll \min\{1-\beta,\,1-\zeta\} \quad . \tag{41}$$

This thin-shell limit displays a strong inverse dependence on the bulk Lorentz factor $\Gamma = 1/\sqrt{1-\beta^2}$ of the expansion, as is evident from Fig. 2: typically $\alpha \sim 2-3$ for EGRET bursts (e.g. see Table 2). This dependence is enhanced by one or two powers of Γ that appear in the determination of R_0. This case is closest to the work of Fenimore, Epstein and Ho (1993), who treat test photons coming from an entire spherical shell (i.e. including the limb regions). As argued in Section 2.1, the major contribution to the optical depth comes from test photons originating in near-axis environs so that the differences between conclusions made using a formula like Eq. (41) and the work of Fenimore et al. (1993) are marginal.

2.3.2. Filled-sphere expansions

The other extreme class of expansions from the point of view of the radial dimension contains filled spheres initially, i.e. thick shells (in the comoving frame) with $\Delta R/R_0 \gg 1-\beta$. Again we shall ignore the impact of narrowing the solid angle down and demand $\Theta_{\rm B} = \pi/2$ here, so that only one term in Eq. (37) contributes to the optical depth. In this limit, inspection of Eq. (37) soon reveals that the dominant contribution to the integral is for $s-1 \lesssim 1-\beta$. Then it follows

that $\lambda \approx -(1-\beta)/(s-1)$, since relativistic expansions with $\beta \approx 1$ are considered here. Choosing $\lambda/(\lambda-1)$ as the integration variable and using the transformation of the hypergeometric function in Eq. (A2) yields a result that is proportional to the integral in Eq. (A4). As in the thin-shell limit, here $\tau_{\gamma\gamma}(\varepsilon_t) \propto (\Delta R)^2$, reflecting the dimensionality of the integrations. The filled sphere limit of Eq. (18) indicates that an observed flux gives a volume-determined photon injection rate $\dot{\mathcal{N}} \propto 1/(\Delta R)^3$, so that the overall expression for the optical depth is a declining function of the expansion thickness: for $\beta \approx 1$, the asymptotic result

$$\tau_{\gamma\gamma}(\varepsilon_t) \;\approx\; \frac{3\sigma_{\rm T}}{4c}\,\frac{d^2}{\Delta R}\,\mathcal{F}\,(1-\beta)^{\alpha+1}\,\varepsilon_t^{\alpha-1}\,(\alpha+3)\,\frac{\mathcal{H}(\alpha)}{2^\alpha}\left[\,\frac{1}{\alpha}+\frac{2}{\alpha-1}\left\{\psi(2\alpha)-\psi(\alpha)-1\right\}\right] \qquad (42)$$

is derived, where $\psi(x)$ is the derivative of the logarithm of the Gamma function, defined in Eq. (A4). Again, a strong dependence on the bulk Lorentz factor of the expansion is evident. The moderate decline of $\tau_{\gamma\gamma}(\varepsilon_t)$ with ΔR reflects the fact that large regions are less compact for a given source luminosity. Note that extremely-filled spheres with $\Delta R > R_0$ are not really discussed in this paper; these seem unlikely to be realized in bursts and require an alternative coupling of length scale to time variability, via $\Delta R = c\Delta t$, as is mentioned below.

2.3.3. Narrow beam expansions

The case of small opening angles of the expansion is also of interest. Since the emphasis here is on axial viewing perspective, this limiting case corresponds to $\zeta \equiv \cos\Theta_{\rm B} \approx 1$. Specifically, this narrow beam limit satisfies $1-\zeta \ll 1-\beta$, so that the reduction in opening angle dominates the causality limitations, and also $1-\zeta \ll \delta \equiv \Delta R/R_0$. However, such an identification with small solid-angles is not sufficient to define narrow beam cases; as will be evident shortly, the size of the opening angle itself is also quite pertinent. The most suitable form of the optical depth for development here is using Eq. (37a) combined with the representation in Eq. (39). The s-integration then consists of a range $1 \le s \le 1/\zeta$ over which the volume is not opening angle-limited, and this contributes of the order of $1-\zeta$ to the optical depth expression in Eq. (37a). However, it turns out that the range $1-\zeta \ll s-1/\zeta \ll 1$ dominates the contribution to the integral. This leads to a simplification for the integral in Eq. (39) for $\mathcal{J}_\alpha(s;\,\beta,\,\zeta)$. Yet the integral is not trivial since the parameter λq_+ is not necessarily small; in fact $-\lambda q_+ \approx s(1-\zeta)(1-\beta)/(s-1)^2$. Reversing the order of integration and using 3.194 of Gradshteyn and Ryzhik (1980) leads to the result that $\tau_{\gamma\gamma}(\varepsilon_t) \propto \dot{\mathcal{N}}\sqrt{1-\zeta}$. This result is subject to the requirements that $\sqrt{1-\zeta} \ll 1-\beta$ and $\sqrt{1-\zeta} \ll \delta$. Clearly the reduction in angular phase space for pair creation is not solid-angle limited, but rather constrained purely by the maximum size of the angle between the momentum vectors of the test and interacting photons — this scales as $\Theta_{\rm B}$. Such a linear dependence on $\Theta_{\rm B}$ is manifested in both this asymptotic limit for Eq. (37a) and the range of its validity. When $\delta \ll \sqrt{1-\zeta}$ then the optical depth in Eq. (37a) no longer behaves like a narrow beam limit, but rather like a thin-shell limit as discussed above, where $\tau_{\gamma\gamma}(\varepsilon_t) \propto \dot{\mathcal{N}}\,\delta^2$.

The other part of the narrow beam calculation relates to the flux normalization factor $\mathcal{F}$ in Eq. (17). Remembering the limitation in Eq. (19), the computation of $\mathcal{F}$ is straightforward, yielding a solid-angle limited flux: $\mathcal{F} \propto \dot{\mathcal{N}}(1-\zeta)$. This intuitively obvious result is applicable only when $1-\zeta \ll 1-\beta$ and $1-\zeta \ll \delta$. Such a solid-angle-limited range differs from the requirements imposed by Eq. (37), thereby complicating the consideration of the narrow beam limit. To aid understanding of this limit, the various dependences of Eq. (17) and Eq. (37), and the resulting behaviour of the overall optical depth, as functions of $\Theta_{\rm B}$ and δ, are listed in Table 1. There, four parameter regimes with $\sqrt{1-\zeta} \ll 1-\beta$ are identified, depending on δ. Three of these regimes are strictly narrow beam limits, while the fourth, for $\delta \ll 1-\zeta$, corresponds to the thin-shell limit in Eq. (41), and is independent of $\Theta_{\rm B}$. For the first two regimes in Table 1, the developments of Eqs. (17) and (37) just mentioned lead to an approximate overall optical depth that can be written as one expression:

$$\tau_{\gamma\gamma}(\varepsilon_t) \;\approx\; \frac{3\sigma_{\rm T}}{2c}\,\frac{d^2}{R_0}\,\mathcal{F}\,\sqrt{\pi}\,\frac{\Gamma(\alpha+1/2)}{\Gamma(\alpha+1)}\,\frac{\mathcal{H}(\alpha)\,[2(1-\beta)+\delta]}{3(1-\beta)^2+3(1-\beta)\delta+\delta^2} \times \frac{(1-\beta)^{\alpha+3/2}}{(1+\beta)^{\alpha+1}}\,\frac{\varepsilon_t^{\alpha-1}}{\sqrt{1-\zeta}} \quad , \qquad \sqrt{1-\zeta} \ll \min\Big\{1-\beta,\,\frac{\Delta R}{R_0}\Big\} \quad , \tag{43}$$

for $\delta = \Delta R/R_0$. This formula encompasses both thin-shell, narrow beam ($\sqrt{1-\zeta} \ll \delta \ll 1-\beta$) and thick-shell, narrow beam ($\sqrt{1-\zeta} \ll 1-\beta \ll \delta$) regimes. Surprisingly, the calculated optical depth actually *increases* when the opening angle closes down, reflecting the *explicit* dependence [see Eqs. (17) and (19)] of the observed flux on the solid-angle of the expansion, combined with the pair production rate explicitly depending only on the angle between the test and interacting photon momenta. Essentially, the photon density in the source increases for constant observed flux as the expansion opening angle is reduced. The resulting optical depth varies only with the thickness of the shell ($\propto 1/\Delta R$) in the regime of thick shell expansions, i.e. for $\Delta R/R_0 \gg 1-\beta$. The third regime in Table 1 requires use of the thin-shell evaluation of $\tau_{\gamma\gamma}/\dot{\mathcal{N}}$, and yields the asymptotic approximation

$$\tau_{\gamma\gamma}(\varepsilon_t) \approx \frac{\sigma_{\rm T}}{4c}\,\frac{d^2}{R_0}\,\mathcal{F}\,\varepsilon_t^{\alpha-1}\,\frac{\mathcal{H}(\alpha)}{\alpha}\,\left(\frac{1-\beta}{1+\beta}\right)^{\alpha}\,\frac{\delta}{1-\zeta} \quad , \qquad 1-\zeta \ll \delta \ll \sqrt{1-\zeta} \ll 1-\beta. \tag{44}$$

This bears an even stronger dependence on the opening angle $\Theta_{\rm B} \approx \sqrt{2(1-\zeta)}$, again rising with increased narrowness of the beam, a property that corresponds to an enhanced mean density of radiation in the expansion. In this case, the phase-space for pair production is not restricted by the opening angle, but rather only by the thinness of the shell, while the flux is still solid-angle limited.

Finally, in concluding the consideration of narrow beam cases, observe that Eq. (43) approximately reproduces the thin shell and filled-sphere forms in Eqs. (41) and (42) when the beam is opened up to $1-\zeta \sim 1-\beta$. For this intermediate (or critical) regime of opening angles, a domain common to all three of the limiting cases discussed so far is achieved when $\Delta R/R_0 \sim 1-\beta$. This locality in phase space corresponds to the so-called "blob" scenario of earlier work (e.g. Krolik and

Pier 1991; Baring 1993; Baring and Harding 1993) on pair production transparency constraints in gamma-ray bursts, a situation that is discussed in Section 3.

2.3.4. Stationary radiation gas

The remaining limiting case of the optical depth is for a $\beta = 0$ or non-relativistic expansion. This is mostly of academic interest as a check on the numerical evaluations that follow, and does not have great physical import for the problem considered in this paper. In fact the result in Eq. (37) does not aptly model stationary gases since we have neglected the limb contributions to the optical depth; these become significant in non-relativistic expansions. Set $\Theta_{\rm B} = \pi/2$ for simplicity. In the $\beta \to 0$ limit, $\lambda \to -2/(s-1)$, which simplifies Eq. (37) somewhat. However, analytic development of the subsequent result is not fruitful, so it is convenient to consider separately the thin and thick shell cases. The limiting result in Eq. (41) was derived without restriction on β, so the limit $\beta \to 0$ can be taken to obtain the optical depth for stationary, thin shell sources. For $\Delta R/R_0 \gg 1-\beta$ a derivation alternative to that in subsection 2.3.2 is requisite. Then the dominant contribution to the integration comes from $s - 1 \ll \delta$. The transformation relation in Eq. (A2) can be used, together with a change of variable to yield a result proportional to both ΔR^2 and the integral in Eq. (A5). The flux is simply evaluated when $\beta = 0$, so that the optical depth for a thick stationary gas is

$$\tau_{\gamma\gamma}(\varepsilon_t) \;\approx\; \frac{3\sigma_{\rm T}}{4c}\,\frac{d^2}{\Delta R}\,\mathcal{F}\,\frac{\mathcal{H}(\alpha)}{1+2\alpha}\left\{1+(\pi-3)\Big[\frac{3}{2(\alpha+1)}\Big]^{9/8}\right\}\varepsilon_t^{\alpha-1} \quad , \quad \frac{\Delta R}{R_0} \gg 1-\beta \quad . \qquad (45)$$

Note that this estimate differs somewhat from results derived for isotropic photons (e.g. Schmidt 1978; Epstein 1985; in particular those that use the formalism of Gould and Schreder 1967), because in this paper we have assumed isotropic *injection* in the comoving frame (in this particular limit the observer's frame), which is not equivalent to radiation isotropy due to radiative transfer in the sphere.

2.4. Numerical computation of the optical depth

The various limiting cases just explored guide the technique for numerical determination of the optical depth, and further act as checks on computational accuracy. The numerics are generally straightforward, and it is expedient to use $s-1$ as an integration variable in Eqs. (17) and (37), and scale quantities in terms of $1-\beta$ to maintain good accuracy for large Lorentz factors. Since the range of integration variable contributing significantly to the two integrals is sometimes quite large, logarithmic sampling of $s-1$ is favoured. Use of the functional form in Eq. (37b) comfortably produces smooth results for $\Theta_{\rm B}$ down to even smaller than 0.01 degrees, so use of the alternative representation in Eq. (39), or a series in $1-\zeta$, is unnecessary for the purposes of this paper.

Numerical determinations of the optical depth formed by the combination of Eqs. (37) and (17) are presented in Fig. 2 for different fractional shell thicknesses $\Delta R/R_0$ illustrating its strong dependence on Γ, and significant dependence on source opening angle only for smaller Γ. The inclusion of $\beta \ll 1$ cases is intended only to provide a general guide to the behaviour of the optical depth (perhaps to order of magnitude accuracy), but this is strictly incorrect since they neglect limb contributions. The quantity actually plotted in Fig. 2 is the scaled optical depth

$$\frac{\tau_{\gamma\gamma}(\varepsilon_t)}{\mathcal{F}} \, \frac{\Delta t\,(\mathrm{ms})}{d^2_{\mathrm{Gpc}}} \left[\varepsilon_t(1+z)\right]^{1-\alpha} \; = \; 1.06 \times 10^{13} \, \frac{c\Delta t}{R_0} \, \mathcal{R}(\alpha;\, \beta,\, \Delta R/R_0) \quad , \tag{46}$$

which is dimensionless since $\mathcal{F}$ is measured in photons per square centimeter per second, where $\mathcal{R}(\alpha;\, \beta,\, \Delta R/R_0)$ is just $\mathcal{H}(\alpha)/(1+\beta)^{1+\alpha}$ times the ratio of the two integrals in Eqs. (37) and (17). Here Δt is the observed source variability timescale, typically in the range of 10^{-3}–1 seconds, inferred, for example, from time histories such as those exhibited in the BATSE 1B catalogue (Fishman et al. 1994), and z is the cosmological redshift of the source (it is set to zero in Fig. 2). The coefficient of this equation clearly defines the optical depth scale for cosmological bursts, and would be 8–10 orders of magnitude smaller for galactic halo sources. A "canonical" spectral index of $\alpha = 2.5$ (see Table 2 for specific values) is chosen in Fig. 2 for simplicity; increasing (reducing) α just increases (lowers) the slope of the curves in the $\Gamma \gg 1$ regimes. Remembering that the energy ε_t is expressed in units of $m_e c^2$, it is evident from Fig. 2 that the maximum observed energies of EGRET sources (see Table 2) imply that Lorentz factors in the range of approximately 50–500 are required to render these bursts optical thin to pair production.

The curves in Fig. 2a clearly delineate three regimes of parameter space in order of increasing bulk Lorentz factor: (i) non-relativistic flows where the optical depth is independent of the expansion speed, (ii) thin-shell expansions ($\Delta R/R_0 \ll 1-\beta$ and $\Gamma \gg 1$), which is the portion of phase space sampled by the work of Fenimore, Epstein and Ho (1993), yielding a strong inverse dependence of $\tau_{\gamma\gamma}$ on Γ, and (iii) at the highest Lorentz factors (i.e. above the break at $(\Delta R/R_0)/(1-\beta) \sim 1$), thick-shell expansions, where the inverse dependence on Γ is slightly stronger (by two powers of Γ: compare Eqs. (41) where $\tau_{\gamma\gamma} \propto (1-\beta)^{\alpha}/R_0$ and (42) where $\tau_{\gamma\gamma} \propto (1-\beta)^{\alpha+1}/\Delta R$). We note that Fenimore, Epstein & Ho (1993) produced an optical depth vs. $\log\Gamma$ plot for their infinitely thin shell analysis that exhibited a dramatic reduction of $\tau_{\gamma\gamma}$ above some critical Lorentz factor. These turnovers were found to be artificial, being caused by a coding error (Fenimore, private communication). The ratio $\Delta R/R_0$ is independent of Γ in Fig. 2a, though other choices are quite plausible. For opening angles $\Theta_{\mathrm{B}} \gtrsim 1/\Gamma$, the ratio $\chi \equiv (\Delta R/R_0)/(1-\beta)$ is the only critical parameter delineating the thin-shell and thick-shell cases, and is intimately related to the the portion of the emission region that is causally-connected to the test photon. As is evident from Eqs. (41) and (42), the optical depth is independent of the thickness of the shell when this parameter is much less than unity, and inversely proportional to ΔR when $\chi \gg 1$; the transition between these regimes is quite gradual. The curves exhibit a lack of dependence on the opening angle Θ_{B} when $\Theta_{\mathrm{B}} \gtrsim \min\{1/\Gamma, (\Delta R/R_0)^{1/2}\}$ (the curves in Fig. 2a are coincident for $\Theta_{\mathrm{B}} = 90^\circ, 10^\circ$, and 1°): this is a consequence of causality dominating geometry in the restriction of the integration phase space. When $\Theta_{\mathrm{B}} \lesssim 1/\Gamma$, the optical depth ($\propto (1-\beta)^{\alpha+3/2}/[\Theta_{\mathrm{B}}\, R_0]$) is actually increased

by the angular reduction of the available phase space, an effect that is particularly evident for non-relativistic expansions. As mentioned in Section 2.3.3, the reason for this increase in optical depth with declining $\Theta_{\rm B}$ is that the pair production rate is proportional to the angle between the test and interacting photons (which is limited linearly by $\Theta_{\rm B}$), while the flux scales as the solid angle (i.e. $\Theta_{\rm B}^2$ when $\Theta_{\rm B} \ll 1$) of the expansion. Hence the density of photons in the source that is inferred for a given flux actually increases as $1/\Theta_{\rm B}$ when $\Theta_{\rm B}$ declines below $1/\Gamma$. In Fig. 2b, where $\Delta R/R_0$ is approaching unity, the thin-shell regime is no longer distinct from the non-relativistic domain so that all relativistic expansions are thick-shell.

The specific choice of $R_0 = \Gamma c \Delta t$ is made in Fig. 2 for simplicity; alternative dependences on Γ are possible, corresponding to different interpretations of source timescales (as discussed in Section 3 below), and these result in only a slightly different appearance from the curves in Fig. 2. The results presented in this subsection are obtained under the assumption that the test photon starts its life at the rear of the expansion; Eq. (40) provides a simple scheme of substitution for Eq. (37) that yields optical depths for arbitrary initial positions of the test photon within the expansion. It is evident that imposing a $\tau_{\gamma\gamma} = 1$ condition on EGRET bursts potentially can map over into both thin and thick shell regimes, depending on the assumed source distance, measured flux and maximum photon energy observed. We note that using a $\tau_{\gamma\gamma} = 1$ criterion for source transparency actually leads to conservative lower bounds for Γ, since significant attenuation is already present when $\tau_{\gamma\gamma} = 1$. This can be easily seen if the spectrum is attenuated by an exponential factor $\exp\{-\tau_{\gamma\gamma}\}$, a common choice. A central consequence of the assumption of an infinite power-law burst spectrum is that the optical depth is an *increasing* (and power-law) function of energy, so that spectral attenuation arises only at high energies; departures from this behaviour will be discussed briefly at the end of the next Section. We remark also that opacity skin effects (which depend on the spatial distribution of photons and therefore are model-dependent) can sometimes render the exponential $\exp\{-\tau_{\gamma\gamma}\}$ a poor descriptor of attenuation, with $1/(1+\tau_{\gamma\gamma})$ perhaps being an improvement for uniformly-distributed photons, leading to broken power-laws rather than exponential turnovers. A variety of signatures of spectral attenuation are possible, particularly if pair cascading is involved, and some of these are illustrated in the work of Baring and Harding (1997).

Undoubtedly the most crucial piece of information to be gleaned from Fig. 2 is that causality minimizes the role of the opening angle $\Theta_{\rm B}$ of the expansion in faster expansions, and specifically that the $\tau_{\gamma\gamma} = 1$ condition will be virtually independent of $\Theta_{\rm B}$ in the range $90^\circ \geq \Theta_{\rm B} \gtrsim 1/\Gamma$ for burst sources. This insensitivity to the angular extent of the expansion is the keystone to elimination of the number problem for cosmological bursts, as is discussed below.

3. BULK LORENTZ FACTORS FOR EGRET SOURCES

The calculations for $\tau_{\gamma\gamma}$ we have performed can readily by applied to gamma-ray bursts detected by EGRET. The pair production optical depth in Eq. (37) depends on the free parameters: Γ, $\Delta R/R_0$, $\Theta_{\rm B}$, d, and on the observed parameters: source flux $\mathcal{F}$ [defined in Eq. (16)], high energy spectral index α [see Eq. (15)], test photon energy ε_t $(= \varepsilon_{\rm MAX})$, and Δt. The burst variability timescale Δt can be used to infer an upper limit on the source size, which we take for the moment to be $R_0 = \Gamma c \Delta t$, based on the apparent size of the expanding shell perpendicular to the light of sight, as seen by a stationary observer (e.g. see Rees, 1966). Alternative size-estimates, such as those that couple the source variability to dimensions along the line of sight to the source, are possible. In addition, measured minimum variability timescales for bursts range from milliseconds in the BATSE range to supersecond values in EGRET data. Motivations for choosing either of these Δt, and also different source size determinations, are discussed below. Both variability timescales are addressed in the results presented here, for the sake of completeness.

The key observable parameters, to be used in the pair production opacity calculations of this paper, are displayed in Table 2 for six of the burst detections by EGRET. Note that there are eleven EGRET bursts in total (Schneid et al. 1996), three of which have insufficient (published) data for the purposes of our analyses; GRB 920622 and GRB 940301 have the required observational parameters in Schneid et al. (1995), but suffer from poor statistics above about 2 MeV. We therefore conservatively opt to study just the most significant six sources of the EGRET population. In Table 2, the fluxes are expressed in observer-friendly units, via $f(1\,{\rm MeV})$, which is just the flux, evaluated at 1 MeV, per MeV energy interval (the flux $\mathcal{F}$ is per $m_e c^2$ at 511 keV). These fluxes are obtained via extrapolations down to 1 MeV of the best-fit power-laws to the time-integrated super-MeV spectral data, and are not necessarily the actual fluxes measured at 1 MeV. Note that both EGRET and COMPTEL parameters are listed for GRB 910601 since this burst was relatively soft and actually had a slightly more significant detection by COMPTEL than by the EGRET TASC in the 3–5 MeV range. We remark that the COMPTEL listings for GRB 910601 (based on Hanlon et al. 1994) differ slightly from those quoted by Baring and Harding (1993) that were obtained from Winkler et al. (1993). As noted in the Table caption, in the computations of this paper we neglect the highest energy (18 GeV) photon detected for GRB 940217. This conservative step is taken because the statistically-limited sample provided by a single photon leads to a large uncertainty in the spectral form at these energies, which is compounded by the lack of contemporaneous spectral information at lower (i.e. sub-MeV) energies (e.g. Hurley et al. 1994); time-resolved spectra of good statistical quality in the super-100 MeV range await future generations of instrumentation. A nice depiction of the relative fluxes and spectra of four of these bursts is given in Hurley (1996).

3.1. Geometries with $\Theta_{\rm B} \sim 1/\Gamma$

Before presenting the results for the bulk Lorentz factor constraints inferred from our optical depth calculations here, it is instructive to first review the results of previous, more primitive bulk motion determinations. As outlined in the Introduction, the earlier work of Krolik and Pier (1991) and Baring (1993), and subsequent papers, considered "blobs" of radiation-emitting material moving at relativistic speeds more-or-less along the line of sight to an observer. The angular extent of these blobs, i.e. the width of the angular distribution of photons as measured in the observer's frame, was assumed to be comparable to $1/\Gamma$, where Γ was the Lorentz factor of the blob ($\Gamma \gg 1$). For such relativistically-moving blobs, the minimum bulk Lorentz factors at redshift z are obtained (i.e. for $\tau_{\gamma\gamma} = 1$) from the result derived by Baring and Harding (1993, corrected in Harding 1994):

$$\Gamma^{1+2\alpha} \gtrsim \frac{(3.83)^{\alpha}\,(1+z)^{\alpha-1}}{3\alpha^{5/3}(4/3+\alpha)^{27/11}}\,\frac{d^2_{\rm kpc}}{\Delta t\,({\rm ms})}\left(\frac{\varepsilon_{\rm MAX}}{1\ {\rm MeV}}\right)^{\alpha-1} f(1\ {\rm MeV}) \quad . \tag{47}$$

Here $f(1\,{\rm MeV})$ is just the source flux evaluated at 1 MeV, per MeV energy interval, and therefore is proportional to $\mathcal{F}$. This formula can be approximately reproduced from Eq. (41) by setting $R_0 \sim \Gamma c\Delta t$. Alternatively the thick shell approximation in Eq. (42) gives more or less the same estimate if $\Delta R \sim c\Delta t/\Gamma$. It therefore follows that the "blob calculation" corresponds to the boundary between thin and thick shell cases where the line-of-sight and transverse (e.g. variability) timescales are comparable. Furthermore, it also coincides with the boundary of narrow beam expansions, namely for $\Theta_{\rm B} \sim 1/\Gamma$, as can be established by setting $1-\zeta = 1-\beta$ in Eq. (43) and choosing intermediate shell thicknesses.

We remark here that the choice of variability timescale for use in the estimation of minimum source bulk Lorentz factors is subjective. The smallest Δt observed in BATSE data (see Fishman et al. 1994) is of the order of milliseconds, and it is quite conceivable that intrinsic source variability occurs on even shorter timescales. Such small Δt were adopted in the work of Baring (1993), Baring and Harding (1993, 1995, 1996) and Harding (1994), and lead to light-crossing time size determinations of $c\Delta t \sim 3\times 10^7\,{\rm cm}$. However, variability in the hard gamma-ray band, i.e. for Comptel and EGRET data, can only be conclusively inferred from more severely photon-limited samples on the order of 0.1 second to 1 second timescales. Hence a conservative approach, adopted for example by Ryan et al. (1994, for GRB 930131) and Winkler et al. (1995, for GRB 940217), uses these longer Δt values in obtaining pair production constraints on bulk motion in bursts. Note that the relative timescales in the different GRB energy bands may not be related at all to intrinsic source properties but merely reflect current instrumental limitations in the time domain. While experimentalists might prefer the conservative variability values, theorists are often motivated to attribute the shortest timescales to regions emitting the highest energies of radiation. This is frequently justifiable in astrophysics, since a whole host of cosmic objects are powered from a central region and thereby generate their most energetic photons closer to the center; such photons would generally be expected to couple to shorter timescales. If a central "powerhouse" is indeed responsible for gamma-ray burst emission (as suggested by Fenimore, Madras and Nayakshin 1996), then

sub-millisecond timescales might accurately reflect the source conditions appropriate to EGRET photons. In contrast, if bursts approximate more closely the class of fireball models that generate the emission we see by impact on the interstellar medium (e.g. Rees and Mészáros 1992, Mészáros and Rees 1993), perhaps through diffusive acceleration of particles at shocks, then the highest energy photons are produced by particles diffusing on the largest scales of the system, and therefore might be expected to have longer variability timescales than photons in the BATSE energy range. To accommodate a variety of perspectives, this paper considers Δt values of 1 ms and 1 second.

The solutions of Eq. (47) for the minimum bulk Lorentz factor $\Gamma_{\rm MIN}$ for the burst parameters of Table 2 are listed in Table 3, for the two different variability timescales, and for four different GRB source distances that are typical of galactic disk, galactic halo, and nearby and distant cosmological populations (though the redshift $z = 0$ is chosen for simplicity). The immediately obvious conclusion is that, except for a disk origin of bursts, relativistic bulk motion is generally inferred for the EGRET sources, because of the detection of energetic photons. The Lorentz factors obtained for cosmological distance scales far exceed those inferred for extragalactic jets in active galaxies. Conversely, Table 3 indicates that isotropic emission cannot be supported in GRBs unless they are quite local, i.e. well within the galactic disk, a conclusion that differs from Schmidt's (1978) early work principally because of the positive EGRET detections in the CGRO era. These estimates for the minimum Γ in bursts are a good first guide to constraints on bulk motion in their emission regions; the refinements of the burst geometries addressed in this paper only modify the estimates in Table 3 by factors of at most a few, as will become evident shortly. We remark that previous versions of these estimates (e.g. Baring 1993, Baring and Harding 1993, Harding 1994, Baring 1995) have sometimes used slightly different observational parameters. Note that a number of entries in the 1 kpc column have $\Gamma_{\rm MIN} = 1$. These actually represent unphysical $\Gamma < 1$ solutions to Eq. (47) that are obtained only because the assumption $\Gamma \gg 1$ is used to derive Eq. (47). Hence $\Gamma_{\rm MIN} = 1$ entries denote regimes where this "blob" constraint breaks down and refinements are needed. It must be emphasized that Eq. (47) and the work of this paper implicitly assume that the GRB spectrum extends above 511 keV in the rest frame of the emission region, so that phase space above pair creation threshold is non-zero.

It is appropriate to remark on a caveat to these results. Given emission observed out to $\varepsilon_{\rm MAX}$, the maximum photon energy in the source rest frame is of the order of $\varepsilon_{\rm MAX}/\Gamma$, which must exceed unity in order to be above pair threshold. Hence the possibility that intrinsic cutoffs could be present in the GRB spectrum anywhere above $\varepsilon_{\rm MAX}$ automatically implies that $\varepsilon_{\rm MAX}$ provides a potential lower bound to Γ. In particular, when the estimate for $\Gamma_{\rm MIN}$ obtained from Eq. (47) exceeds $\varepsilon_{\rm MAX}$, it is quite possible that pair creation never occurs at all, since opacity for photons of energy $\varepsilon_{\rm MAX}$ occurs through interactions with photons *at even higher energies*, for which there is no observational evidence. Cases with values of $\Gamma_{\rm MIN}/\varepsilon_{\rm MAX}$ greater than unity generally arise only for small Δt and at cosmological distances (see Table 3: GRB910601 is a perfect example). In such instances, these cutoff considerations become quite relevant, and it becomes necessary to take $\varepsilon_{\rm MAX}$ as the estimate for the minimum Lorentz factor Γ. Since values of $\varepsilon_{\rm MAX}$ between 1

and 10 MeV in the collection of EGRET bursts are a marker of fainter or steeper spectrum bursts, i.e. probably reflecting the observational limitations of EGRET, it is quite realistic to develop bulk motion estimates based Eq. (47), in the belief that many (if not most) bursts emit at energies much higher than 100 MeV.

3.2. Generalized Geometries

Generalizing from Eq. (47) to the expansion geometries considered in this paper, a pair production transparency condition is obtained by setting the optical depth that is obtained from Eqs. (37) and (17) equal to unity, i.e. effectively reading off abscissa values for chosen ordinates from curves like those in Fig. 2. Since the expressions for the optical depth and flux from the expansion involve integrals with integrands that depend on the bulk Lorentz factor, the solutions for $\Gamma_{\rm MIN}$ roots to $\tau_{\gamma\gamma} = 1$ must be solved iteratively: we adopt a bisection technique. The minimum bulk Lorentz factors $\Gamma_{\rm MIN}$ for EGRET burst sources that result from our pair production transparency calculations in Eqs. (37) and (17) are depicted in Fig. 3 as functions of the fractional shell thickness $\Delta R/R_0$. This illustration limits shell thicknesses to regimes where $\Delta R/R_0 \leq 1$, since R_0 is tied to the time variability via $R_0 = \Gamma c \Delta t$, and this coupling becomes inappropriate for $\Delta R \gtrsim R_0$ regimes, where $\Delta R \sim c\Delta t$ is a more apt choice. Again the source parameters from Table 2 are used, and results are presented for large expansion half-angles, $\Theta_{\rm B} = 90^\circ$, variability timescales of $\Delta t = 1\,{\rm ms}$, and source distances of 100 kpc and 1 Gpc that represent galactic halo and cosmological burst scenarios, respectively. Cosmological redshift modifications, which depend on the choice of cosmology, are neglected for simplicity. All of the twelve curves in the four panels exhibit similar behaviour, with $\Gamma_{\rm MIN}$ being independent of $\delta = \Delta R/R_0$ when $\delta \lesssim 1-\beta$, the so-called thin-shell limit, and $\Gamma_{\rm MIN}$ declining roughly as δ^{-1} for $\delta \gg 1-\beta$ when the filled-sphere regime is realized. These dependences on $\Delta R/R_0$ appear explicitly in the asymptotic forms in Eqs. (41) and (42). Domains where $\Delta R/R_0 > 1$ (i.e. for a true filled sphere) are not depicted since they are unlikely to be encountered in gamma-ray bursts. The values of $\Gamma_{\rm MIN}$ obtained when $\Delta R/R_0 \sim 1-\beta$ (i.e. the transition regions) are comparable to those listed in Table 3 for all bursts; this reflects the broad applicability of the constraint in Eq. (47) that is the hallmark of the so-called "blob" calculation.

The curves in Fig. 3 generally concur with the global trends of increasing $\Gamma_{\rm MIN}$ for higher $\varepsilon_{\rm MAX}$ and/or declining spectral index α. Yet the cross-over of two curves in the lower left-hand panel exemplifies how the expansion geometry can complicate trends, and generate non-monotonic behaviour in $\varepsilon_{\rm MAX}$ or α. For comparison, Fig. 4 reproduces the bottom right panel of Fig. 3, but for a variability timescales of $\Delta t = 1\,{\rm sec}$. The curves resemble those of Fig. 3. However, at these cosmological distances, $\Gamma_{\rm MIN}$ is reduced from the corresponding values in Fig. 3 solely because the large Δt dilutes the density of internal photons inferred for the source. Again a cross-over of curves arises, indicating that non-monotonicity of $\Gamma_{\rm MIN}$ in $\varepsilon_{\rm MAX}$ and α does not belong exclusively to galactic halo scenarios. Note that the uncertainties in the observational quantities that are listed in Table 2 are as large as around 10%. These lead to uncertainties in the $\Gamma_{\rm MIN}$ determinations for

both these figures of the order of 20%, which are largely masked by the ranges of $\Gamma_{\rm MIN}$ produced by varying model parameters. Hence further consideration of experimental uncertainties is omitted from this paper. Note also that the results we have presented have assumed that the test photons in the source start from the rear of the expansion. This maximizes the computed optical depths, implying that it is possible to lower our estimates for $\Gamma_{\rm MIN}$ somewhat. Permitting test photons to be emitted throughout the source will perhaps lower the mean optical depth by a factor of 2 or so, leading to a reduction of $\Gamma_{\rm MIN}$ of around 15%. Hence the detailed consideration of the distribution of *test* photons is neglected in this paper as this will only have a minor impact on the $\Gamma_{\rm MIN}$ obtained.

The results presented in Figs. 3 and 4 clearly define the behaviour of our $\Gamma_{\rm MIN}$ solutions for large opening angles, but obviously do not address the entire available phase space for model parameters. Hence in Fig. 5 we depict the variations of $\Gamma_{\rm MIN}$ with expansion opening angle $\Theta_{\rm B}$ for fixed $\Delta R/R_0$. These curves unequivocally demonstrate how insensitive $\Gamma_{\rm MIN}$ is to $\Theta_{\rm B}$ when $\Theta_{\rm B} \gtrsim 3\Delta R/R_0$, i.e. for a range from modestly small $\Theta_{\rm B}$ up to 90°. Note that such a substantial range is realized for the adopted values of $\Delta R/R_0$, chosen to correspond to the transition between thin-shell and thick-shell regimes. This insensitivity, whose important implications for cosmological models are discussed at the end of this subsection, is a principal conclusion of this paper. The values of $\Gamma_{\rm MIN}$ at the intercept with the right hand side axis of each panel in Fig. 5 are just those obtained by vertically slicing the plots in the bottom two panels of Fig. 3 at the appropriate value of $\Delta R/R_0$. For $\Theta_{\rm B} \ll \Delta R/R_0$, power-law asymptotic behaviour of $\Gamma_{\rm MIN}$ is observed in the Figure, with the dependence being easily deduced (for $1-\beta \ll \Delta R/R_0$) from Eq. (43): $\Gamma_{\rm MIN} \propto \Theta_{\rm B}^{-1/(2\alpha+3)}$. This is a very weak dependence (for α in the range 2–3 typical of EGRET bursts) on $\Theta_{\rm B}$, generated by the strong variation of the optical depth with Γ.

It is quite instructive to augment these plots by summarizing the behaviour of the optical depth results with phase space diagrams using well-chosen variables. This can be achieved in an enlightening manner for both observational and theoretical (i.e. model) phase space parameters via contour plots, i.e. exhibiting curves of constant Γ $(=\Gamma_{\rm MIN})$ that satisfy the criterion $\tau_{\gamma\gamma}=1$ for the pair production optical depth. First of all, we focus on the space of observational parameters given by the maximum energy observed, $\varepsilon_{\rm MAX}$, and the EGRET spectral index α, both being listed in Table 2 for EGRET bursts. Fixing the observed flux and the source time variability at the "canonical" values of $f(1\ {\rm MeV}) = 3\,{\rm cm}^{-2}\ {\rm sec}^{-1}\ {\rm MeV}^{-1}$ and $\Delta t = 1\,{\rm ms}$, respectively, the resulting contour plot is shown in Fig. 4. These contours, which represent lower boundaries to regions of opacity (i.e. $\tau_{\gamma\gamma}>1$), display a number of trends that are hallmarks of the optical depth properties of the relativistically expanding radiation gas.

First, $\varepsilon_{\rm MAX}$ is an increasing function of α. This arises because, for the particular values of $f(1\ {\rm MeV})$, Δt and Γ chosen, solutions with $\varepsilon_{\rm MAX} < \Gamma$ are always realized. For such solutions, the test photons at energy $\varepsilon_{\rm MAX}$ interact with photons near pair production threshold in the CM frame, i.e. with photons of energy around $\varepsilon_{\rm MAX}/\Gamma^2$ $(<1\,{\rm MeV})$ in the observer's frame. Since the optical depth is held constant (i.e. unity), and the flux is pinned at 1 MeV, thereby providing a

"pivot point" in the spectrum, increasing α then raises the number of interacting photons (with energies below 1 MeV) so that $\varepsilon_{\rm MAX}$ must correspondingly be increased to compensate. This trend solely finds its origin in the realization of an $\varepsilon_{\rm MAX} < \Gamma$ branch of solutions. As $\alpha \to \infty$, the energy of the interacting photons must approach the pivot point, i.e. 1 MeV. Hence the $\varepsilon_{\rm MAX}$ curves asymptotically approach $\sim \Gamma^2$ as α becomes very large, behaviour that is conspicuous in the galactic halo cases in Fig. 6. In the particular examples shown, $\varepsilon_{\rm MAX}$ drops off rapidly as α approaches unity, a singularity of these curves [e.g. see Eq. (37)]. The monotonic increase of $\varepsilon_{\rm MAX}$ with α can be inverted to yield a declining tendency if an $\varepsilon_{\rm MAX} > \Gamma$ solution branch can be encountered, so that interacting photons are always above the pivot point at 1 MeV. This occurs when the product $f(1\ {\rm MeV})\, d^2/\Delta t$ is small enough, i.e. forcing $\varepsilon_{\rm MAX}$ higher for given Γ and α [e.g. see Eq. (37)]. Then the contours would rise rapidly as α approached unity, but still asymptote to roughly a Γ^2 dependence for $\alpha \to \infty$. This situation is more likely to arise for $\Delta t = 1\,{\rm sec}$ variability timescales. Note that the larger values of $f(1\ {\rm MeV}) d^2/\Delta t$ in the cosmological cases in Fig. 6 yield stronger dependences of $\varepsilon_{\rm MAX}$ on α, primarily because these cases generally have larger "lever arms" for the interacting photons (at energy $\sim \varepsilon_{\rm MAX}/\Gamma^2$) around the pivot point at 1 MeV.

The dependence of $\varepsilon_{\rm MAX}$ on Γ is very closely given by the blob calculation in Eq. (47), namely $\varepsilon_{\rm MAX} \propto \Gamma^{-(1+2\alpha)/(\alpha-1)}$. For example, doubling Γ at $\alpha = 2$ in either of the galactic halo or cosmological cases yields an increase of around 29.4, which is close to the "blob" estimate of 32. Similarly, doubling Γ at $\alpha = 3$ in either of the galactic halo or cosmological cases yields an increase of around 11.2, which is very close to the "blob" estimate of 11.3. For fixed α, these amplification ratios are independent of the source distance d, since d just forms part of the proportionality constant for the relationship between $\varepsilon_{\rm MAX}$ and Γ. Another trend that is apparent in Fig. 6 is that $\varepsilon_{\rm MAX}$ declines with decreasing $\delta = \Delta R/R_0$. The variation of $\varepsilon_{\rm MAX}$ with δ is depicted using the light solid curves for the galactic halo scenario, with the $\delta = 0.3(1-\beta)$ and $\delta = 3(1-\beta)$ cases visually defining a band around the $\delta = 1-\beta$ case (the behaviour for cosmological source distances is similar). When δ is reduced, the average density of photons within the source increases, pushing the optical depth up. Hence, to compensate, $\varepsilon_{\rm MAX}$ must also decline with δ, so defining the observed trend; in Figs. 3 and 4, this effect forces $\Gamma_{\rm MIN}$ to increase when $\varepsilon_{\rm MAX}$ is held constant. From those figures, it is evident that when $\delta \ll 1-\beta$, the thin-shell limit produces insensitivity of the optical depth to δ, a feature that is also apparent in Fig. 6, for which the $\delta = 0.3(1-\beta)$ curves are more proximate to the $\delta = 1-\beta$ ones than are the $\delta = 3(1-\beta)$ cases. Finally, we note that the value of $f(1\ {\rm MeV})$ for each of the EGRET bursts that are depicted as points in Fig. 6 differs from the chosen canonical value. Hence for those sources with higher $f(1\ {\rm MeV})$ (GRB 910503 and GRB 910814), the exhibited curves should be slid down somewhat to visualize the situation (i.e. infer bulk Lorentz factors) appropriate for these bursts. Likewise, for the remaining EGRET bursts, the curves should be moved upwards to deduce Γ values that are consistent with the results depicted in Figs. 3 and 4.

The theoretical phase space contour plot is presented in Fig. 7, which exhibits curves of constant Γ that satisfy the criterion $\tau_{\gamma\gamma} = 1$, in the space defined by the opening angle $\Theta_{\rm B}$ and the fractional shell thickness $\delta = \Delta R/R_0$. We focus on regimes where $\Delta R/R_0 \leq 1$ since, as mentioned above, we have tied R_0 to the time variability via $R_0 = \Gamma c\Delta t$, a coupling that becomes inappropriate for $\Delta R \gtrsim R_0$ regimes, where $\Delta R \sim c\Delta t$ is a more apt choice. The large range of $\Theta_{\rm B}$ is chosen intentionally to present the information relating to the reduction of expansion opening angles that is omitted from earlier considerations, such as in Figs. 3 and 4. For all contours, the maximum energy and spectral index were set at $\varepsilon_{\rm MAX} = 100\,{\rm MeV}$ and $\alpha = 2.21$, respectively, and the variability timescale Δt and the flux $f(1\ {\rm MeV})$ at 1 MeV are representative of EGRET-like sources. These parameters were tuned somewhat to obtain a maximum of informational content in the figure, so that other choices of parameters can lead to some variations in contour shape. Remembering the general trend of a reduction in $\tau_{\gamma\gamma}$ with increasing $\Theta_{\rm B}$, the contours in Fig. 7 clearly represent upper boundaries to regions of opacity (i.e. $\tau_{\gamma\gamma} > 1$).

A number of prominent features appear in this phase space plot. Foremost among these are the vertical portions of the $\Gamma = 10$ and $\Gamma = 250$ contours, present when the opening angles are significant. These define regimes where the optical depth is independent of $\Theta_{\rm B}$, and both thin-shell and thick-shell regimes that are well-described by the asymptotic formulae in Eqs. (41) and (42) can be realized. It is precisely this upper region of the $\Theta_{\rm B}$-δ diagram that is probed in solutions depicted in Figs. 3 and 4. The virtual independence of the optical depth to δ observed in those solutions for $\Gamma_{\rm MIN}$ manifests itself in Fig. 7 as an extreme sensitivity of the position of any vertical sections of the contours to the choice of Γ (or $\varepsilon_{\rm MAX}$ or α). This sensitivity therefore produces a low density of contours in the upper left hand portion of Fig. 7, so that contours possessing vertical sections occupy a minority of cases if broad ranges of $\Theta_{\rm B}$ are considered. Note also that low values of Γ are obtained only in the upper right of the figure. However, since values of $\Delta R/R_0$ greater than unity are unrealistic, it becomes clear that for this choice of $\varepsilon_{\rm MAX}$ and α, only values of $\Gamma \gtrsim 5$ are attained. This signifies the general property of these calculations that *relativistic bulk motions are always inferred* unless $\varepsilon_{\rm MAX}$ is not too much greater than 1 MeV.

The narrow beam (i.e. $\Theta_{\rm B} \lesssim 0.01$) portion of the parameter space exhibits distinctive power-law dependences, with $\Theta_{\rm B}$ rising as $\sqrt{\delta}$ when δ is very small, and declining as $1/\delta$ when δ exceeds $1-\beta$. This asymptotic behaviour can be deduced with the aid of Eqs. (43) and (44). Table 1 identifies four parameter regimes, three of which are relevant to narrow beam considerations, the other being the domain of large $\Theta_{\rm B}$ discussed in the previous paragraph. Eq. (44) is pertinent to the lower left hand portion of Fig. 7; contours of unit optical depth thereby defining the dependence $\Theta_{\rm B} \propto \delta^{1/2}/\Gamma^{\alpha+1/2}$ (for $R_0 = \Gamma R_v$). In this limit, doubling Γ decreases $\Theta_{\rm B}$ by around a factor of 6.54 for $\alpha = 2.21$, regardless of the assumed distance to the source. The lower right of the figure is described by the thick shell (i.e. $\delta \gg 1-\beta$) limit of Eq. (43), which yields contours with $\Theta_{\rm B} \propto \delta^{-1}\Gamma^{-(2\alpha+2)}$; doubling Γ in this limit reduces $\Theta_{\rm B}$ by a factor of 343 for $\alpha = 2.21$, behaviour that is borne out in Fig. 7. The third asymptotic domain is defined by the thin-shell limit of Eq. (43), yielding contours approaching a limit with $\Theta_{\rm B} \propto \Gamma^{-(2\alpha+2)}$, independent of δ.

This domain is almost attained at the broad peaks of the contours that remain always in the narrow beam (i.e. lower) portion of phase space, particularly for the $\Gamma = 40$ and $\Gamma = 1000$ cases in the figure. These three limiting forms can be written explicitly as (for $\Gamma \gg 1$ and $R_0 = \Gamma R_v$):

$$\Theta_{\rm B} \sim \begin{cases} \mathcal{F}\,\dfrac{\sigma_{\rm T}}{c}\,\dfrac{d^2}{R_v}\,\mathcal{H}(\alpha)\,\dfrac{3\sqrt{\pi}\,\Gamma(\alpha+1/2)}{2^{2\alpha+3}\,\Gamma(\alpha+1)}\,\dfrac{\varepsilon_{\rm MAX}^{\alpha-1}}{\Gamma^{2\alpha+4}}\,\dfrac{1}{\delta}\,, & \sqrt{1-\zeta} \ll 1-\beta \ll \delta\,, \\ \mathcal{F}\,\dfrac{\sigma_{\rm T}}{c}\,\dfrac{d^2}{R_v}\,\mathcal{H}(\alpha)\,\dfrac{\sqrt{\pi}\,\Gamma(\alpha+1/2)}{2^{2\alpha+1}\,\Gamma(\alpha+1)}\,\dfrac{\varepsilon_{\rm MAX}^{\alpha-1}}{\Gamma^{2\alpha+2}}\,, & \sqrt{1-\zeta} \ll \delta \ll 1-\beta\,, \\ \left\{\mathcal{F}\,\dfrac{\sigma_{\rm T}}{c}\,\dfrac{d^2}{R_v}\,\dfrac{\mathcal{H}(\alpha)}{2^{2\alpha+1}\alpha}\right\}^{1/2}\,\dfrac{\varepsilon_{\rm MAX}^{(\alpha-1)/2}}{\Gamma^{\alpha+1/2}}\,\delta^{1/2}\,, & 1-\zeta \ll \delta \ll \sqrt{1-\zeta} \ll 1-\beta\,. \end{cases} \tag{48}$$

These asymptotic formulae are depicted as thin, light, dotted lines in Fig. 7 for the $\Gamma = 40$ galactic halo case, clearly indicating how the contours closely approach these in the appropriate ranges of δ. The lowest Γ examples in Fig. 7 for each of the galactic halo and cosmological scenarios do not realize thin shell portions of phase space without assuming significant opening angles $\Theta_{\rm B}$. This feature marks the general property that low Γ curves occupy the upper right corner of the $\Theta_{\rm B} - \delta$ diagram, a domain where the thick shell parts of the solutions in Figs. 3 and 4 are appropriate. Other trends relevant to the $\Theta_{\rm B} - \delta$ diagram include a general reduction of $\Theta_{\rm B}$ with increases in α or decreases in $\varepsilon_{\rm MAX}$.

This concludes the survey of observational and theoretical parameter space. In view of the extensive presentation of results in this section, it is important to highlight the implication of this work that is most salient for gamma-ray bursts. The principal conclusion of our work (expounded in brief in Baring and Harding 1996, with a preliminary version given in Harding and Baring 1994), is that $\Gamma_{\rm MIN}$ is quite insensitive to the choice of $\Theta_{\rm B}$ when $\Theta_{\rm B} \gtrsim 1/\Gamma_{\rm MIN}$, behaviour that can be inferred from Figs. 2. This result arises because causality restricts the available phase space for pair production interactions more effectively than does the expansion opening angle $\Theta_{\rm B}$, when $\Theta_{\rm B} \gtrsim 1/\Gamma_{\rm MIN}$; it has profound repercussions for gamma-ray burst models. For such source models, the principal advantage (e.g. Krolik and Pier 1991) of restricting $\Theta_{\rm B}$ to small values like $1/\Gamma$ is a lower (solid angle-reduced) luminosity at the source for a given observed flux. However, the number of non-repeating sources must then be a factor $\Theta_{\rm B}^{-2} \sim \Gamma^2$ higher in order to account for the observed burst rate. In the case of cosmological GRBs, this factor could be as high as 10^6 for the values of $\Gamma_{\rm MIN}$ determined here, which is unacceptably large for many models, particularly those that involve neutron star–neutron star or neutron star–black hole mergers (Paczyǹski 1986; Eichler et al. 1989; Narayan, Piran and Shemi 1991; Mészáros & Rees 1992), failed Type 1b supernovae (Woosley 1993) and rapid spin-down of high-field millisecond pulsars (Usov 1992). This defined the commonly-perceived "number problem" for cosmological bursts. Clearly, in view of the results of our analysis, this problem is a non-issue, since imposition of small opening angles $\Theta_{\rm B}$ in order to satisfy pair production transparency in EGRET bursts is not necessary. Hence, causality restrictions to the optical depth differ so little between $\Theta_{\rm B} = 90^\circ$ and $\Theta_{\rm B} \sim 1/\Gamma$ cases that burst population statistical requirements can comfortably be satisfied without resorting to beamed expansion geometries. Of course, opening up the expansion angle then amplifies the energetics requirements accordingly, so

that model development must still meet the needs of acceptable bursting rates and energy budgets. In such considerations, it is evident from the work presented here that pair production constraints will play only a secondary role in determining such model requirements, becoming involved purely through the evaluation of permissible Lorentz factors for bulk motion in gamma-ray bursts.

3.3. Discussion

The choice of coupling the scale of the expansion to the variability timescale via transverse dimensions is subjective, though it is widely adopted in applications of bulk relativistic motion in astrophysics. Other choices are possible, such as using burst or subpulse durations (e.g. Fenimore, Madras and Nayakshin 1996) and/or relating these to longitudinal dimensions in the source. It is fitting to outline the reasons for adhering to our preference. Suppose that timescales larger than the variability time Δt, for example the burst duration T_d, are used as the observational diagnostic of the source size. For uniform expansions, as we have assumed, the geometrical appearance of the "look-back" volume forces the time profile to maintain a well-defined shape ($[t/T_d]^{-\alpha-2}$ for spectral index $\alpha = 2$) that mimics the so-named FRED (fast rise, exponential decay) profile (Fenimore, Madras and Nayakshin 1996). This profile necessarily has a width of the order of T_d under these assumptions, so that its smooth, decaying shape is inconsistent with the vast majority of burst time histories. Temporal consistency can therefore be attained only if the appropriate observational timescale is of the order of the variability time δt, so that the burst comprises a multitude of shells, or perhaps if a single shell is "patchy" in the transverse dimension. The latter possibility still produces time profiles that do not match many burst histories, so that one is compelled to adopt the many-shell proposition, perhaps produced by a central engine, as advocated by Fenimore, Madras and Nayakshin (1996). The timescale that is then appropriate is Δt, precisely our choice, though the value of this depends on whether BATSE or EGRET variabilities are used (as discussed in Section 3.1 above).

The issue of whether the variability should be tied to transverse or longitudinal source dimensions remains to be addressed. Since Δt is always close to the threshold of temporal resolution of any of the CGRO instruments BATSE, Comptel and EGRET, it is appropriate to assume that *measured* variability is actually an upper bound to the source variability. If we opt to relate this to the direction transverse to the line of sight to the observer, then the inequality $R_0/\Gamma \lesssim c\Delta t$ follows, and it is customary to take the equality to specify R_0. By the same token, if dimensions along the line of sight are preferred, this inequality is replaced by $R_0/\Gamma^2 \lesssim c\Delta t$. A consistent description of the expansion can only be obtained when both of these inequalities are satisfied, which obviously occurs when the more-constraining $R_0/\Gamma \lesssim c\Delta t$ is adopted. This motivates our choice of coupling the variability to the transverse dimension; tying it to the line-of-sight direction is insufficiently restrictive. Notwithstanding, the difference between these two choices is merely one Lorentz factor in the optical depth [compared with around five or six imposed by the spectrum: see Eq. (43)], to which the estimates of $\Gamma_{\rm MIN}$ are quite insensitive: opting for $R_0/\Gamma^2 \lesssim c\Delta t$ reduces $\Gamma_{\rm MIN}$ by

factors of the order of two or less. Other possibilities for choosing the scale of the expansion exist, such as $\Delta R = c\Delta t$, and these are discussed at length in the temporal analysis of Fenimore, Madras and Nayakshin (1996). Note that fixing $\Delta R = c\Delta t$ with either $R_0 \sim \Gamma c\Delta t$ or $R_0 \sim \Gamma^2 c\Delta t$ yields $\Delta R/R_0 \ll 1$, comfortably in the phase space covered by Fig. 7. The essential point that should be emphasized is that these subjective alternatives probe details of the expansion microstructure that are beyond the purpose of this analysis, and are largely peripheral to it, primarily because of the relative insensitivity of the $\Gamma_{\rm MIN}$ estimates to these choices. The principal conclusions of this paper, including the insensitivity of the optical depth to the expansion opening angle $\Theta_{\rm B}$, are guaranteed regardless of such variations on our assumptions.

One question that naturally arises when obtaining estimates for the bulk Lorentz factors via pair production constraints is why the values of $100-1000$ obtained here for cosmological bursts are of the same order as those obtained from fireball expansions (e.g. Paczyǹski 1986; Shemi & Piran 1990; Rees & Mészáros 1992) of enormous initial optical depths. This similarity is no coincidence. The bulk motions attained by the adiabatic expansion phase of pure electron-positron (pair) fireballs yield Lorentz factors Γ that saturate at some value corresponding more or less to the "freeze-out" of pair production, i.e. the epoch of free expansion is approximately marked by the onset of pair production transparency. For cosmological bursts, where the luminosities can be of the order of $L \sim 10^{49} - 10^{50}\,{\rm erg/sec}$ and the energy deposition can be larger than $10^{51}\,{\rm ergs}$, the optical depth is roughly $L\sigma_{\rm T}/(R\,m_e c^2)/\Gamma^5$ (e.g., for E^{-2} spectra) and can be $10^{10}/R_{10}$ or larger for $\Gamma = 1$, where R_{10} is the size of the fireball at the end of the epoch of opacity in units of $10^{10}\,{\rm cm}$. This optical depth can be reduced to unity by relativistic beaming with Γ in the range of $100-1000$ when $R_{10} \sim 1$. Since the Lorentz factor attained during the fireball "acceleration phase" scales roughly as its radius (e.g. Paczyǹski 1986; Piran, Shemi and Narayan 1993), then it follows that values of a freeze-out radius of $R_{10} \sim 1$ would correspond to $\Gamma \sim 100-1000$ for fireballs initiated in regions of diameter $10^7 - 10^8\,{\rm cm}$. These $10^{10}\,{\rm cm}$ scalelengths for the onset of expansion transparency are comparable to those used for $R_0 = \Gamma c\Delta t$ in this paper, thereby explaining the similarity of our estimates for $\Gamma_{\rm MIN}$ to the Lorentz factors of fireball-initiated relativistic expansions.

The results we have presented focus on the energy range appropriate to EGRET detections of gamma-ray bursts. There are now ongoing programs for searches for bursts at TeV energies, specifically the target of opportunity monitoring of BATSE localization error boxes by the Whipple air Čerenkov experiment, using the rapid response that is facilitated by the BACODINE alert network (Barthelmy et al. 1995). While these efforts have failed to provide any positive TeV detections so far, probably due to the fact that Whipple's sensitivity threshold still inhibits any possibility of detection for all but the very brightest of bursts (see Connaughton et al. 1995 for a discussion of the current Whipple sensitivity), the prospect of large field of view monitoring of the sky by the air Čerenkov water tank detector MILAGRO (e.g. Yodh 1996) in the very near future, promotes the extension of our bulk motion estimates to the TeV energy range. Such considerations also anticipate future space missions like GLAST, which will span the 10 MeV–200 GeV range. Obviously, increasing $\varepsilon_{\rm MAX}$ to TeV-type energies would tend to push estimates of the bulk Lorentz

factor up, in order to suppress pair creation. To explore the implications of TeV-emitting bursts sources for estimates of $\Gamma_{\rm MIN}$, we computed the infinite power-law "blob" calculation solutions to Eq. (47), and depicted them in Fig. 8, as a function of the spectral index α_h. It is sufficient to focus on this simplest of cases, noting that the complicating effects of expansion geometry mirror those considered at lower maximum energies.

In the figure, the cosmological cases exhibited the expected trend of a dramatic increase in $\Gamma_{\rm MIN}$ for flatter spectra, a consequence of the enhanced supply of interacting photons at $\sim \Gamma^2/\varepsilon_{\rm MAX}$ (generally well above 511 keV) for lower values of α_h. For typical EGRET source spectral indices, in the range 2–3, $\Gamma_{\rm MIN}$ is indeed an increasing function of $\varepsilon_{\rm MAX}$. However, for $\alpha_h < 1$, this behaviour is reversed, with $\Gamma_{\rm MIN}$ declining with $\varepsilon_{\rm MAX}$, because the optical depth in Eq. (47) is then a decreasing function of $\varepsilon_{\rm MAX}$. Note that in the figure, the galactic halo case ($d = 100\,{\rm kpc}$) displays a comparative insensitivity of $\Gamma_{\rm MIN}$ to α_h. This insensitivity arises because the energies ($\sim \Gamma^2/\varepsilon_{\rm MAX}$) of the photons interacting with those at $\varepsilon_{\rm MAX}$ are generally relatively near the pivotal energy of 511 KeV, where the source flux is pinned. In Fig. 8, the source flux f at 511 keV is typical of BATSE burst detections; for this flux, the MILAGRO experiment will be sensitive to bursts with $\alpha_h \lesssim 2.6$, a dividing line that is marked in the figure. Hence, only bright, flat spectrum sources like GRB 910503 provide good candidates for potential detections at TeV energies by MILAGRO, and for that matter Whipple. GLAST will have the capability of spanning the EGRET and sub-TeV energy ranges. This extension of $\Gamma_{\rm MIN}$ estimates to $\varepsilon_{\rm MAX}$ values in the TeV range of course assumes that bursts intrinsically emit at such high energies. Note that for the cosmological case, such intrinsic burst emission is also subject to pair creation in collisions with photons supplied by radiation fields external to the burst, for example the infrared background (Stecker and De Jager 1996, Mannheim, Hartmann and Funk 1996). This type of attenuation is strongly dependent on the redshift of the source, so that sources at 1 Gpc would be strongly attenuated at 1 TeV, while those at 100 Mpc would be transparent. Such external attenuation considerations are beyond the scope of this paper, and are examined in detail by Mannheim, Hartmann and Funk (1996).

The analysis of this paper has made the expedient assumption that the burst spectra are infinite power-laws, with the spectrum matching that observed by EGRET. This, of course assumes that the turnovers seen at sub-MeV energies in BATSE data are immaterial to pair production calculations. The relevance of spectral curvature below the EGRET range to attenuation studies depends upon the energies of the photons that interact with the test photons at $\varepsilon_t = \varepsilon_{\rm MAX}$, which generally are around $\Gamma^2/\varepsilon_{\rm MAX}$ in the stationary observer's reference frame for infinite power-laws, as discussed just above. Clearly, low energy spectral paucity (relative to EGRET-range power-laws) at around $\Gamma^2/\varepsilon_{\rm MAX}$ limits contributions near threshold so that phase space near the pair production threshold is inaccessible, and the process is pushed into the Klein-Nishina regime: the optical depth drops accordingly. Hence MeV and sub-MeV spectral curvature plays a role in opacity determinations when $\Gamma^2/\varepsilon_{\rm MAX} \lesssim 1$, a situation that manifests itself at galactic halo (or even galactic disk) distances for most of the EGRET bursts, as is evident from an inspection of Tables 2 and 3. Consequently, regimes of transparency may become possible at high energies in galactic bursts, so that the range

of opacity becomes finite. These issues are discussed in detail in Baring and Harding (1997), where it is demonstrated that realistic broad-band GRB spectra may yield broad absorption troughs (and also other spectral forms such as shelfs) in the 1 GeV – 1 TeV range of bursts spectra in galactic halo sources, distinctive spectral features whose existence or otherwise could be probed by experiments such as GLAST, Whipple and MILAGRO. Note however, that for cosmological sources, the inferred Γs are so high that $\Gamma^2/\varepsilon_{\rm MAX}$ always exceeds unity and the infinite power-law calculations presented here are always quite appropriate. As a result, the optical depth is then always monotonically increasing in $\varepsilon_{\rm MAX}$, so that only simple (exponential or power-law) spectral turnovers are possible. Hence, Baring and Harding (1997) postulated that such distinguishable spectral structure may provide a means of discriminating between a galactic or cosmological origin for gamma-ray bursts, an enticing prospect for the high energy astrophysics community.

4. CONCLUSION

In this paper, we have presented our extension of pair production transparency calculations in relativistically expanding gamma-ray burst sources to quite general geometries, including shells of finite thickness and arbitrary opening angle. This work includes an extensive analytic reduction of the optical depth from a quintuple integral to a single integral in the special, but quite broadly applicable, case of observing photons only along the axis of the expansion. Such a reduction is extremely expedient for opacity and transparency considerations, providing the reliable and numerically-amenable analytic expressions in Eqs. (17) and (37) that completely describe the pair production optical depth. We determine that the minimum bulk Lorentz factor $\Gamma_{\rm MIN}$ for the EGRET sources to be optically thin up to the maximum energies observed, i.e. display no spectral attenuation, is only moderately dependent on the shell thickness and virtually independent of its opening solid angle if $\Theta_{\rm B} \gtrsim 1/\Gamma_{\rm MIN}$. This insensitivity to $\Theta_{\rm B}$, which is a consequence of the strong impact that causality has on the available interaction phase space, relieves the commonly-perceived number problem for non-repeating sources at cosmological distances: it is not necessary to invoke small $\Theta_{\rm B}$ to effect photon escape. This negation of the number problem for a wide range of expansion geometries is the principal conclusion of this paper, and is an important result for specific cosmological burst models. The values of Γ obtained, typically of the order of 10–30 for halo bursts and $\gtrsim 100$ for sources of cosmological origin, depend only moderately on the choice of GRB timescale used to determine the expansion size. Our new limits on required expansion velocity for given source geometries will significantly aid the placing of realistic constraints on gamma-ray burst source models.

We thank Brenda Dingus and Jennifer Catelli for many discussions about EGRET burst data, and Ed Fenimore and Jim Ryan for numerous conversations concerning gamma-ray bursts. This work was funded, in part, by the Compton Gamma-Ray Observatory Guest Investigator Program.

A. APPENDIX

PROPERTIES OF THE HYPERGEOMETRIC FUNCTION $\mathcal{G}_\alpha(z)$

In the integrand of the expression for the pair production optical depth, Eq. (37), appears the hypergeometric function

$$\mathcal{G}_\alpha(z) \;\equiv\; \int_0^1 dq\,\frac{(1-q)^{2\alpha}}{(1-zq)^{\alpha+1}} \;=\; \frac{1}{1+2\alpha}\,F(\alpha+1,\,1;\,2\alpha+2;\,z) \quad . \tag{A1}$$

This can be represented by the alternative hypergeometric form

$$\mathcal{G}_\alpha(z) \;=\; \frac{1}{1+2\alpha}\,\frac{1}{1-z}\,F(\alpha+1,\,1;\,2\alpha+2;\,z/[z-1]) \quad , \tag{A2}$$

using the transformation formula 9.131.1 of Gradshteyn and Ryzhik (1980).

The argument of $\mathcal{G}_\alpha(z)$ is either λ or $\sigma\lambda$, which can be derived from Eq. (36). It is clear that for $s \geq 1$, λ attains values within a range $-\infty < \lambda < \lambda_{\rm max}$, with $\lambda_{\rm max} = \beta/(1+\beta)$ (note that $d\lambda/ds > 0$). Clearly the condition $\zeta < 1$ renders σ less than unity, so that $\sigma\lambda$ is also bounded by the range $(-\infty,\,\beta/(1+\beta)]$. It follows that there are two natural ways to evaluate $\mathcal{G}_\alpha(z)$ for the purposes of this paper, both using the series expansion (9.100 of Gradshteyn and Ryzhik, 1980):

$$F(\alpha+1,\,1;\,2\alpha+2;\,z) \;=\; 1 + \frac{\alpha+1}{2\alpha+2}\,z + \frac{(\alpha+1)(\alpha+2)}{(2\alpha+2)(2\alpha+3)}\,z^2 + \ldots \quad . \tag{A3}$$

When $|z| < 1$, this series can be used directly with convergence as rapidly as the geometric series $\sum_n (z/2)^n$. When $-\infty < z < -1$, the alternative form for $\mathcal{G}_\alpha(z)$ in Eq. (A2) can be used, where $1/2 < z/(z-1) < 1$; the series in Eq. (A3) with the substitution $z \to z/(z-1)$ then also converges like the geometric series $\sum_n (z/2[z-1])^n$, i.e. with the same rapidity. With this scheme, computation of $\mathcal{G}_\alpha(z)$ to high accuracy is quick.

Note that as $s \to 1$, $\lambda \to -\infty$. Using the representation in Eq. (A2) and also Eq. (36), it is clear that in this limit $(1+2\alpha)\mathcal{G}_\alpha(\lambda)$ approaches $F(\alpha+1,\,1;\,2\alpha+2;\,1)/(1-\lambda)$, and therefore becomes approximately proportional to $s-1$. It follows that the integrand in Eq. (37) is finite as $s \to 1$.

Also of use in this paper, specifically in the determination of the optical depth in the limit of filled spherical expansions, is the integral identity

$$\int_0^1 dz\,z\,\mathcal{G}_\alpha(z) \;=\; \frac{1}{\alpha} + \frac{2}{\alpha-1}\Big\{\psi(2\alpha) - \psi(\alpha) - 1\Big\} \quad , \quad \psi(x) \;=\; \frac{d}{dx}\Big\{\log_e \Gamma(x)\Big\} \quad , \tag{A4}$$

for use in $\beta \approx 1$ situations. This can be established using the integral representation of $\mathcal{G}_\alpha$ in Eq. (A1), then reversing the order of integration and performing the z-integration analytically. An integration by parts then enables the use of identity 3.231.5 of Gradshteyn and Ryzhik (1980), and the result ensues. The finite rational series for $\psi(x+n) - \psi(x)$ was also used in manipulating

Eq. (A4), and for integer α it can be used to obtain rational values for these integrals. For $\beta \ll 1$ cases of initially filled spherical expansions, the integral

$$\int_0^1 \frac{dz}{2-z}\,\mathcal{G}_\alpha(z) \;=\; \int_0^{\pi/2} d\theta\,\theta\,\cos^{2\alpha}\theta \;\approx\; \frac{1}{1+2\alpha}\left\{1+(\pi-3)\left[\frac{3}{2(\alpha+1)}\right]^{9/8}\right\} \qquad \text{(A5)}$$

is needed. The identity is established by using the transformation 9.134.1 in Gradshteyn and Ryzhik (1980) for the hypergeometric function in Eq. (A1), changing to an integration variable of $[z/(2-z)]^2$, using the integral representation for general hypergeometric functions in 9.111 of Gradshteyn and Ryzhik (1980), and then reversing the order of integration. The integral, when multiplied by $1+2\alpha$, is only weakly dependent on α, and the simple approximation obtained in Eq. (A5) is accurate to better than 1% for $0<\alpha<1/2$ and better than 0.1% for $1/2<\alpha<10$.

REFERENCES

Band, D., et al. 1993, *Ap. J.* 413, 281.

Baring, M. G. 1993, *Ap. J.* 418, 391.

Baring, M. G. 1994, *Ap. J. Suppl.* 90, 899.

Baring, M. G. 1995, in *Currents in High Energy Astrophysics,* eds. Shapiro, M. M., Silberberg, R. and Wefel, J. P. (Kluwer, Dordrecht) p. 21

Baring, M. G. and Harding, A. K. 1993, in *Proc. 23rd ICRC* 1, 53.

Baring, M. G. and Harding, A. K. 1995, *Adv. Space Res.,* 15(5), 153.

Baring, M. G. and Harding, A. K. 1996, in *Gamma-Ray Bursts,* eds. Kouveliotou, C., Briggs, M. F., and Fishman, G. J. (AIP Conf. Proc. 384, New York) p. 724.

Baring, M. G. and Harding, A. K. 1997, *Astrophys. J. (Lett.)* 481, L85.

Barthelmy, S. D, et al. 1995, *Astr. Sp. Sci.* 231, 235.

Briggs, M. F. et al. 1996, in *Gamma-Ray Bursts,* eds. Kouveliotou, C., Briggs, M. F., and Fishman, G. J. (AIP Conf. Proc. 384, New York) p. 335.

Catelli, J. R. et al. 1996,in *Gamma-Ray Bursts,* eds. Kouveliotou, C., Briggs, M. F., and Fishman, G. J. (AIP Conf. Proc. 384, New York) p. 185.

Connaughton, V. et al. 1995, in Proc. 24th ICRC (Rome), Vol. II, p. 96.

Dingus, B. L. 1995, *Astr. Sp. Sci.* 231, 187.

Dingus, B. L., et al. 1994, in *Gamma-Ray Bursts,* eds. Fishman, G. J., Hurley, K. and Brainerd, J. J. (AIP Conf. Proc. 307, New York) p. 22

Eichler, D., Livio, M., Piran, T., and Schramm, D. N. 1989, *Nature* 340, 126.

Epstein, R. I. 1985, *Ap. J.* 297, 555.

Fenimore, E. E., Epstein, R. I. and Ho, C. 1992, in *Gamma-Ray Bursts,* eds. Paciesas, W. S. and Fishman, G. J., (AIP Conf. Proc. 265, New York) p. 158

Fenimore, E. E., Epstein, R. I. and Ho, C. 1993, *Astron. Astr. Supp.* 97, 59.

Fenimore, E. E., Klebesadel, R. W. & Laros, J. G. 1996, *Ap. J.* 460, 964.

Fenimore, E. E., Madras, C. & Nayakshin, S. 1997, *Ap. J.* 473, 998.

Fishman, G. J., et al. 1994, *Ap. J. Suppl.* 92, 229.

Goodman, J. 1986, *Astrophys. J. (Lett.)* 308, L47.

Gould, R. J. and Schreder, G. P. 1967, *Phys. Rev.* 155, 1404.

Gradshteyn, I. S. and Ryzhik, I. M. 1980, *Table of Integrals, Series and Products*, (Academic Press, New York)

Hakkila, J., et al. 1995, *Ap. J.* 454, 134.

Hanlon, L. O., et al. 1994, *Astron. Astr.* 285, 161.

Harding, A. K. 1994, in *Proc. 2nd Compton Symp.,* ed. Fichtel, C., et al., (AIP Conf. Proc. 304, New York), p. 30

Harding, A. K. and Baring, M. G. 1994, in *Gamma-Ray Bursts,* eds. Fishman, G. J., Hurley, K. and Brainerd, J. J. (AIP Conf. Proc. 307, New York) p. 520

Hurley, K., et al. 1994, *Nature* 372, 652.

Hurley, K. 1996, in *TeV Gamma-Ray Astrophysics,* eds. Völk, H. J. and Aharonian, F. A. (Kluwer, Dordrecht) p. 43.

Jauch, M. M., and Rohrlich, F. 1980, *The Theory of Photons and Electrons* (2nd edn. Springer, Berlin)

Krolik, J. H. and Pier, E. A. 1991, *Ap. J.* 373, 277.

Kwok, P. W. et al. 1993, in *Compton Gamma-Ray Observatory*, eds. Friedlander, M., Gehrels, N., and Macomb, D. (AIP Conf. Proc. 280, New York) p. 855

Mannheim, K., Hartmann, D. & Funk, B. 1996, *Ap. J.* 467, 532.

Meegan, C., et al. 1992, *Nature* 355, 143.

Meegan, C., et al. 1996, *Ap. J. Suppl.* 106, 65.

Mitrofanov, I. G. 1995, *Astr. Sp. Sci.* 231, 103.

Mészáros, P. & Rees, M. J. 1992, *Ap. J.* 397, 570.

Mészáros, P. & Rees, M. J. 1993, *Ap. J.* 405, 278.

Narayan, R., Piran, T., & Shemi, A. 1991, *Astrophys. J. (Lett.)* 379, L17.

Nemiroff, R. J., et al. 1994, *Ap. J.* 423, 432.

Nolan, P. L. et al. 1983, in *Positron-Electron Pairs in Astrophysics,* eds. Burns, M. L., Harding, A. K., and Ramaty, R., (AIP Conf. Proc. 101, New York) p. 59

Norris, J. P., et al. 1994, *Ap. J.* 424, 540.

Paczyński, B. 1986, *Astrophys. J. (Lett.)* 308, L43.

Piran, T. & Shemi, A. 1993, *Astrophys. J. (Lett.)* 403, L67.

Piran, T., Shemi, A. & Narayan, R. 1993, *Mon. Not. R. astr. Soc.* 263, 861.

Rees, M. J. 1966, *Nature* 211, 468.

Rees, M. J. & Mészáros, P. 1992, *Mon. Not. R. astr. Soc.* 258, 41P.

Ryan et al. 1994, *Astrophys. J. (Lett.)* 422, L67.

Rybicki, G. B. and Lightman, A. P. 1979, *Radiative Processes in Astrophysics* (Wiley, New York)

Schaefer, B. E., et al. 1992, *Astrophys. J. (Lett.)* 393, L51.

Schaefer, B. E., et al. 1994, *Ap. J. Suppl.* 92, 285.

Schmidt, W. K. H. 1978, *Nature* 271, 525.

Schneid, E. J., et al. 1992, *Astron. Astr. (Lett.)* 255, L13.

Schneid, E. J., et al. 1995, *Ap. J.* 453, 95.

Schneid, E. J., et al. 1996, in *Gamma-Ray Bursts,* eds. Kouveliotou, C., Briggs, M. F., and Fishman, G. J. (AIP Conf. Proc. 384, New York) p. 253.

Share, G. H., et al. 1986, *Adv. Space Res.* 6(4), 15.

Shemi, A. & Piran, T. 1990, *Astrophys. J. (Lett.)* 365, L55.

Sommer, M., et al. 1994, *Astrophys. J. (Lett.)* 422, L63.

Stecker, F. W. & De Jager, O. C. 1996, *Space Sci. Rev.* 75, 401.

Stepney, S., and Guilbert, P. W. 1983, *Mon. Not. R. astr. Soc.* 204, 1269.

Svensson, R. 1987, *Mon. Not. R. astr. Soc.* 227, 403.

Usov, V. V. 1992, *Nature* 357, 472.

Weaver, T. A. 1976, *Phys. Rev. A* 13, 1563.

Winkler, C. et al. 1993 in *Proc. Compton Observatory Symposium,* eds. Friedlander, M., Gehrels, N. and Macomb, D. J. (AIP Conf. Proc. 280, New York) p. 845.

Winkler, C. et al. 1995, *Astron. Astr.* 302, 765.

Woosley, S. E. 1993, *Ap. J.* 405, 273.

Yodh, G. B. 1996, *Space Sci. Rev.* 75, 199.

Zdziarski, A. A. 1984, *Astron. Astr.* 134, 301.

TABLE 1

Optical Depth Dependence on δ and $\Theta_{\rm B}$ for Narrow Beams

Regimes of δ for $\Theta_{\rm B} \ll 1-\beta$	$\mathcal{F}/\dot{\mathcal{N}}$ Eq. (17)	$\tau_{\gamma\gamma}/\dot{\mathcal{N}}$ Eq. (37)	$\tau_{\gamma\gamma}$
$\Theta_{\rm B}^2 \ll \Theta_{\rm B} \ll 1-\beta \ll \delta$	$\delta^3\,\Theta_{\rm B}^2$	$\delta^2\,\Theta_{\rm B}$	$\dfrac{1}{\delta\,\Theta_{\rm B}}$
$\Theta_{\rm B}^2 \ll \Theta_{\rm B} \ll \delta \ll 1-\beta$	$\delta\,\Theta_{\rm B}^2$	$\delta\,\Theta_{\rm B}$	$\dfrac{1}{\Theta_{\rm B}}$
$\Theta_{\rm B}^2 \ll \delta \ll \Theta_{\rm B} \ll 1-\beta$	$\delta\,\Theta_{\rm B}^2$	δ^2	$\dfrac{\delta}{\Theta_{\rm B}^2}$
$\delta \ll \Theta_{\rm B}^2 \ll \Theta_{\rm B} \ll 1-\beta$	δ^2	δ^2	constant

Note.— The proportionalities, of the optical depth $\tau_{\gamma\gamma}$ and the two factors $\mathcal{F}/\dot{\mathcal{N}}$ and $\tau_{\gamma\gamma}/\dot{\mathcal{N}}$ contributing to it, to the expansion parameters $\delta = \Delta R/R_0$ and $\Theta_{\rm B}$, specifically in the limit of narrow beam expansions. Remember that in the text, $\zeta = \cos\Theta_{\rm B}$ so that $1-\zeta \sim \Theta_{\rm B}^2/2$, and various regimes of shell thickness or thinness are described in the left-hand column.

TABLE 2
PARAMETERS FOR ENERGETIC GAMMA-RAY BURSTS

GRB	Detecting Instrument	$\varepsilon_{\rm MAX}$ (MeV)	α	$f(1\ {\rm MeV})$ ($\rm cm^{-2}sec^{-1}MeV^{-1}$)
910503	EGRET	170	2.2 ± 0.2	8.71 ± 0.49
910601	EGRET	3.5	3.7 ± 0.2	0.98 ± 0.08
910601	COMPTEL	5.0	2.8 ± 0.2	0.50 ± 0.10
910814	EGRET	60	2.8 ± 0.2	13.5 ± 0.85
930131	EGRET	1000	2.0 ± 0.3	1.95 ± 0.26
940217	EGRET	3380[1]	2.5 ± 0.1	0.36 ± 0.03
950425	EGRET	120	1.93 ± 0.04	1.62 ± 0.09

NOTE.— The maximum energy $\varepsilon_{\rm MAX}$ of detection, the high energy spectral index α, and the (measured or extrapolated) source *photon* flux at 1 MeV for six bursts observed by EGRET. The EGRET detections are from Schneid et al. (1992: GRB 910503), Kwok et al. (1993: GRBs 910601 and 910814), Sommer et al. (1994: GRB 930131), Hurley et al. (1994: GRB 940217) and Catelli et al. (1996 GRB 950425). The COMPTEL measurement of GRB 910601 (see Hanlon, et al. 1994) is included because it was seen at a higher energy than the EGRET detection of this source, and is used in the estimates for lower bounds to Γ in Table 3. [1]The famous 18 GeV photon from GRB 940217 was omitted because it was not contemporaneous with any emission below 100 MeV.

TABLE 3
LOWER BOUNDS FOR Γ IN ENERGETIC GAMMA-RAY BURSTS

GRB	Δt	$\Gamma_{\rm MIN}$ 1 kpc	100 kpc	100 Mpc	1 Gpc	Maximum distance for isotropic emission
910503 (E)	1 ms	2.9	16	199	460	49 pc
910601 (C)	1 ms	1.0	3.8	31	61	1160 pc
910814 (E)	1 ms	3.1	12	101	203	24 pc
930131 (E)	1 ms	2.8	17	276	694	79 pc
940217 (E)	1 ms	4.2	19	195	419	13 pc
950425 (E)	1 ms	1.6	11	188	486	297 pc
910503 (E)	1 s	1.0	4.5	56	130	1.6 kpc
910601 (C)	1 s	1.0	1.3	11	22	37 kpc
910814 (E)	1 s	1.1	4.4	35	71	0.76 kpc
930131 (E)	1 s	1.0	4.4	69	174	2.5 kpc
940217 (E)	1 s	1.3	6.2	62	133	0.43 kpc
950425 (E)	1 s	1.0	2.6	45	117	9.4 kpc

NOTE.— The estimated minimum bulk Lorentz factor $\Gamma_{\rm MIN}$ from Eq. (47), and the maximum source distance that permits isotropic emission, for the six GRBs detected by EGRET, assuming that two-photon pair production does not influence the spectrum below the maximum detected energy $\varepsilon_{\rm MAX}$. The observed spectral index α below $\varepsilon_{\rm MAX}$, as well as the source power-law flux f(1 MeV) at 1 MeV are given in Table 2 (E labels use EGRET data and C indicates use of COMPTEL data); the EGRET power-law fits were extrapolated down to 1 MeV where necessary to define the normalization measure f(1 MeV). At 1 kpc, $\Gamma_{\rm MIN} = 1$ entries represent $\Gamma_{\rm MIN} < 1$ solutions to (i.e. the breakdown of) Eq. (47). Estimates for each burst are given on the two timescales Δt typical of source variability and subpulse duration, as seen by BATSE. Note that source redshifts are set to $z = 0$ in order to avoid a choice of cosmology.

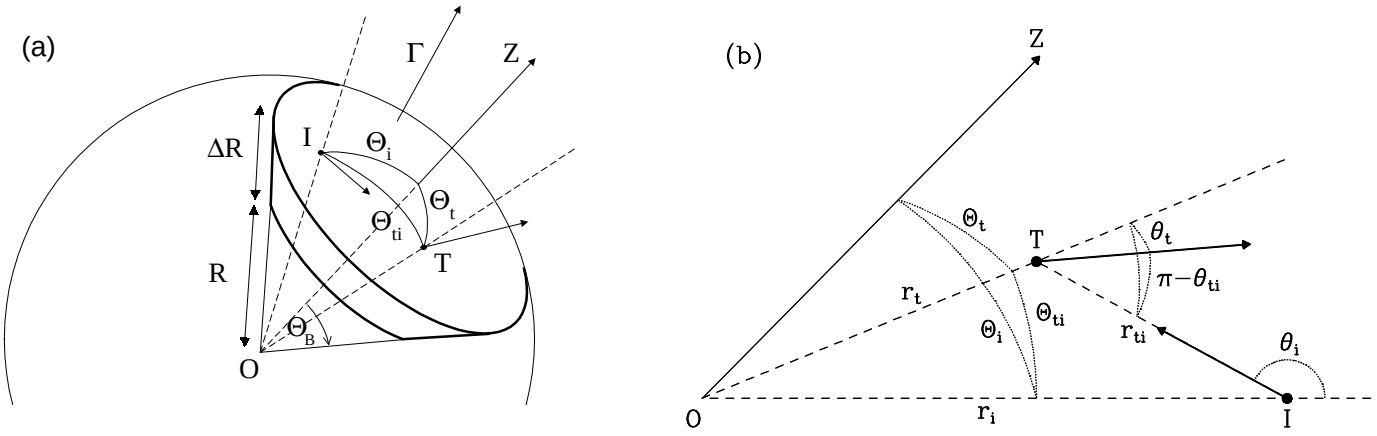

Fig. 1.— (a) A depiction of the source geometry for the relativistic expansions of bulk Lorentz factor Γ considered in this paper. The emission region is at all times a conical sector of a spherical shell with half-angle $\Theta_{\rm B}$. At some time t the inner radius of the shell is given by R, while the thickness of the shell is always ΔR. The test or observable photon is marked by T, and it can interact via $\gamma\gamma \to e^+e^-$ with other (so-called interacting) photons at typical position I. The angles their position vectors (from the origin O of the expansion) make with the axis OZ of the expansion are Θ_t and Θ_i, respectively; the angle subtended by these vectors at the origin is Θ_{ti}. (b) A depiction of the spatial and angular variables, as defined in the text, that are relevant to the analysis of pair production in expanding burst sources. OZ represents the axis of the expansion and generally is not co-planar with the plane (OTI) formed by the positions of the test (T) and interacting (I) photons and the origin (O) of the expansion. The two photon momentum vectors (heavy lines) have an angle θ_{ti} between them and define a third plane that is generally not co-planar with OTI. The "angles of non-radiality" of the test and interacting photons are θ_t and θ_i, respectively, and Θ_{ti} defines the angle subtended at the origin by the positions of the two photons. The labelled distances are $r_t = |\overline{OT}|$, $r_i = |\overline{OI}|$ and $r_{ti} = |\overline{TI}|$.

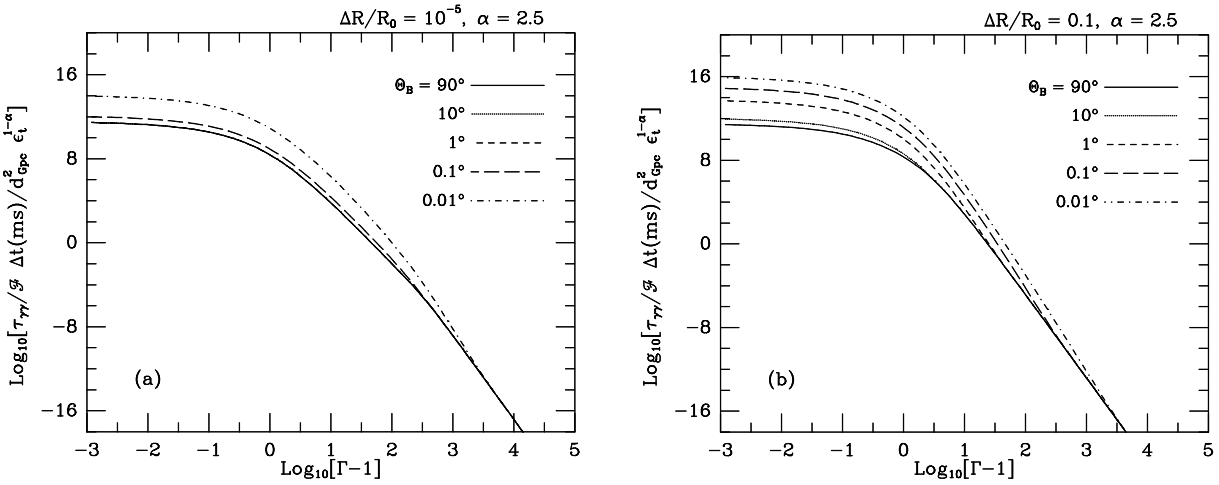

Fig. 2.— The optical depth $\tau_{\gamma\gamma}(\varepsilon_t)$ of test photons to pair production, scaled as in Eq. (46), but for redshift $z = 0$, as a function of bulk Lorentz factor Γ for different opening angles $\Theta_{\rm B}$ of the expansion, as labelled, and for shell fractional thicknesses (a) $\Delta R/R_0 = 10^{-5}$ and (b) $\Delta R/R_0 = 10^{-1}$. The curves are obtained for a typical EGRET source spectral index of $\alpha = 2.5$ and for $R_0 = \Gamma c \Delta t$ (discussed in the text). The scaling distance is chosen to illustrate typical optical depths of cosmological bursts, however the curves are easily translated down by around 8 orders of magnitude if a galactic halo hypothesis is preferred.

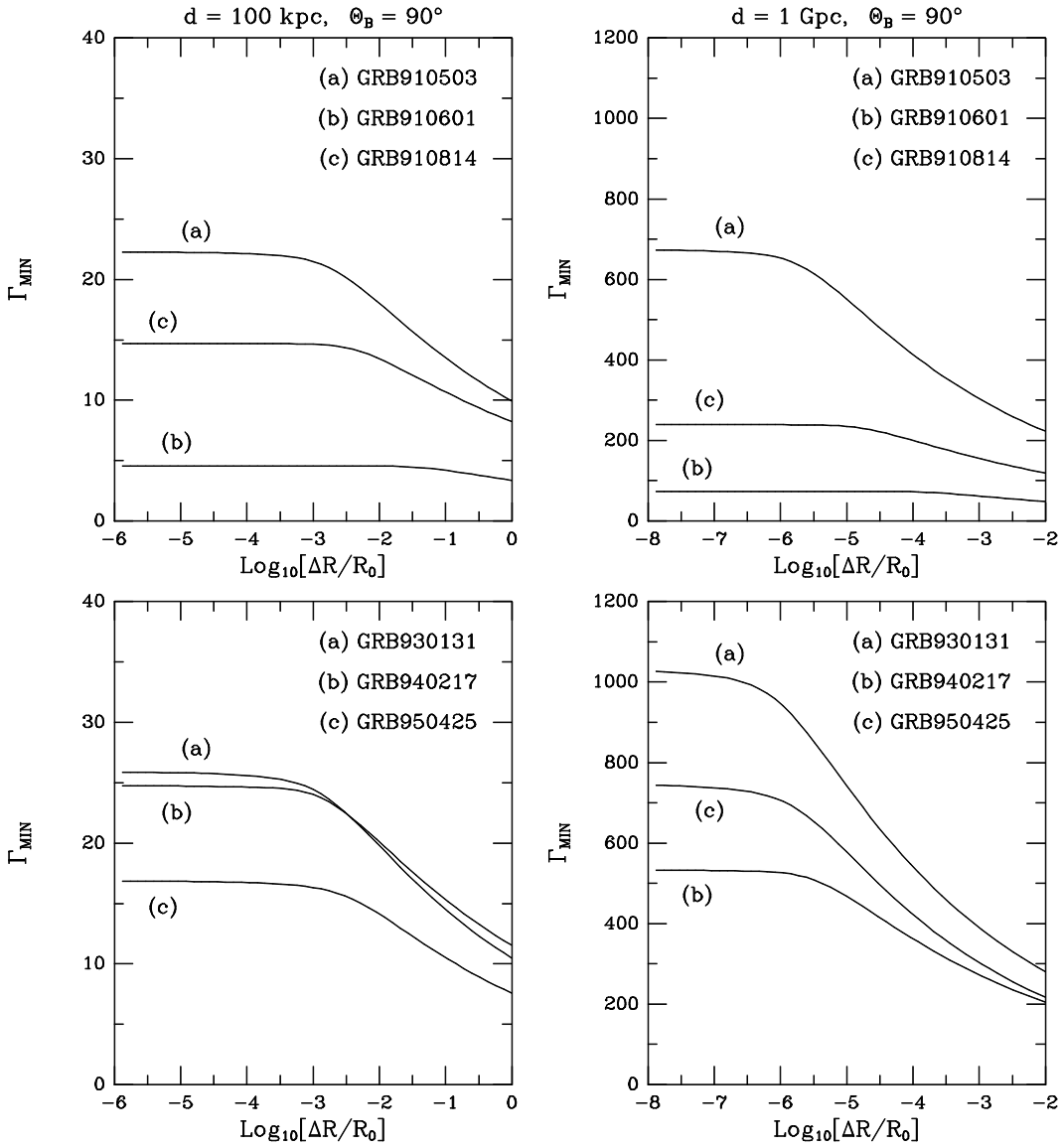

Fig. 3.— The minimum bulk Lorentz factor $\Gamma_{\rm MIN}$ for six EGRET GRBs, as obtained from the pair production condition $\tau_{\gamma\gamma}(\varepsilon_t) = 1$ in Eq. (37). Here ε_t is the maximum energy $\varepsilon_{\rm MAX}$ detected by EGRET; values of $\varepsilon_{\rm MAX}$ and other observational parameters are listed in Table 2 (Comptel data are used for GRB 910601, as in Table 3). The top two panels consider the first three EGRET bursts, while the bottom three are for the most significant of more recent events. Results are shown for two different source distances, $d = 100\,{\rm kpc}$ (left-hand panels) and $d = 1\,{\rm Gpc}$ (right panels), corresponding to galactic halo and cosmological scenarios, respectively. The expansion opening half-angle is set to be $\Theta_{\rm B} = 90^\circ$, and the variability timescale is $\Delta t = 1\,{\rm ms}$. Flat portions of the curves define the thin-shell limit $\Delta R/R_0 \ll 1 - \beta$, while the complementary sloping portions correspond to thick-shell expansions.

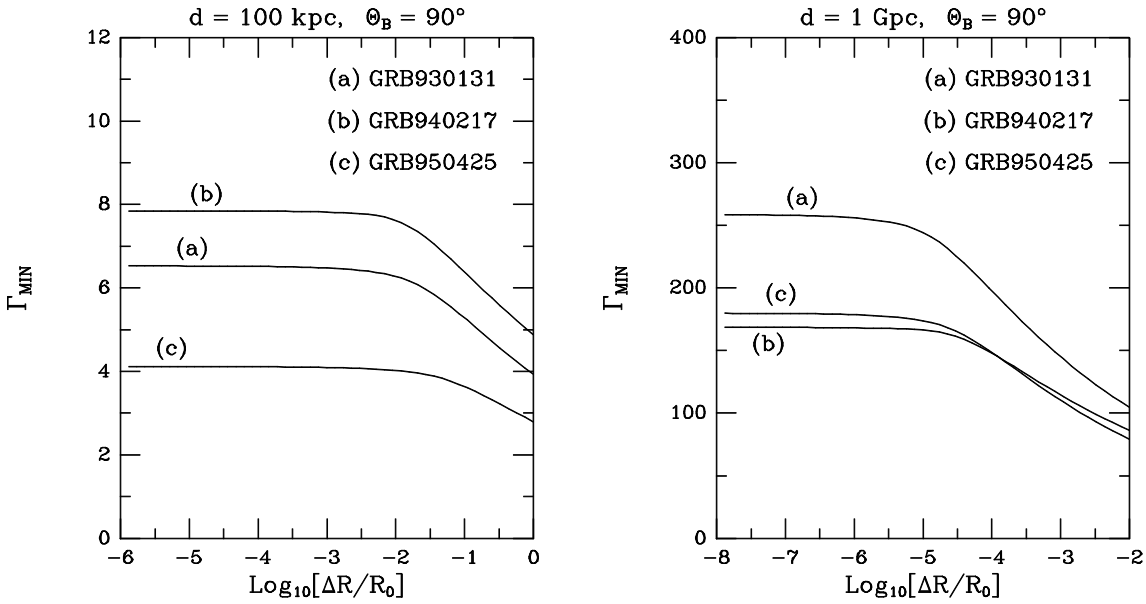

Fig. 4.— The minimum bulk Lorentz factor $\Gamma_{\rm MIN}$ for the most recent three of the six EGRET bursts depicted in Fig. 3, but now for $\Delta t = 1$ second and $d = 100$ kpc (left hand panel) and $d = 1$ Gpc (right hand side), to illustrate the effect of lengthening Δt. Again, the curves represent $\tau_{\gamma\gamma}(\varepsilon_t) = 1$ solutions to Eq. (37), and source parameters are taken from Table 2. Comparison with the bottom panels of Fig. 3 reveals that the $\Gamma_{\rm MIN}$ are reduced significantly for these much longer variability timescales, however the dependence on Δt is nevertheless somewhat weak.

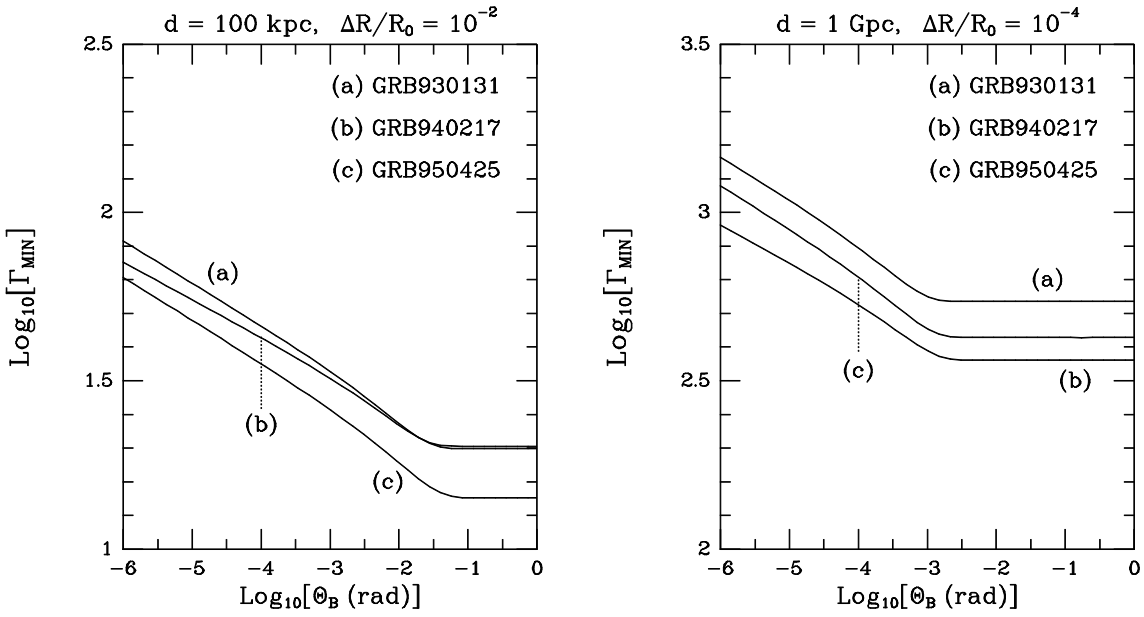

Fig. 5.— The minimum bulk Lorentz factor $\Gamma_{\rm MIN}$ for the most recent three of the six EGRET bursts depicted in Fig. 3, for $\Delta t = 1$ second, but now as a function of the expansion opening angle $\Theta_{\rm B}$. The left hand panel is for $d = 100$ kpc and $\Delta R/R_0 = 10^{-2}$ and the right hand side depicts the cosmological case of $d = 1$ Gpc and $\Delta R/R_0 = 10^{-4}$; the choices of $\Delta R/R_0$ correspond to transitions between the thin and thick-shell regimes. Again, the curves represent $\tau_{\gamma\gamma}(\varepsilon_t) = 1$ solutions to Eq. (37), and source parameters are taken from Table 2. Clearly evident is the independence of $\Gamma_{\rm MIN}$ on opening angle when $\Theta_{\rm B} \gg \Delta R/R_0$, and a very weak power-law dependence [whose slope depends on a burst's spectral index α via Eq. (43)] for $\Theta_{\rm B} \ll \Delta R/R_0$.

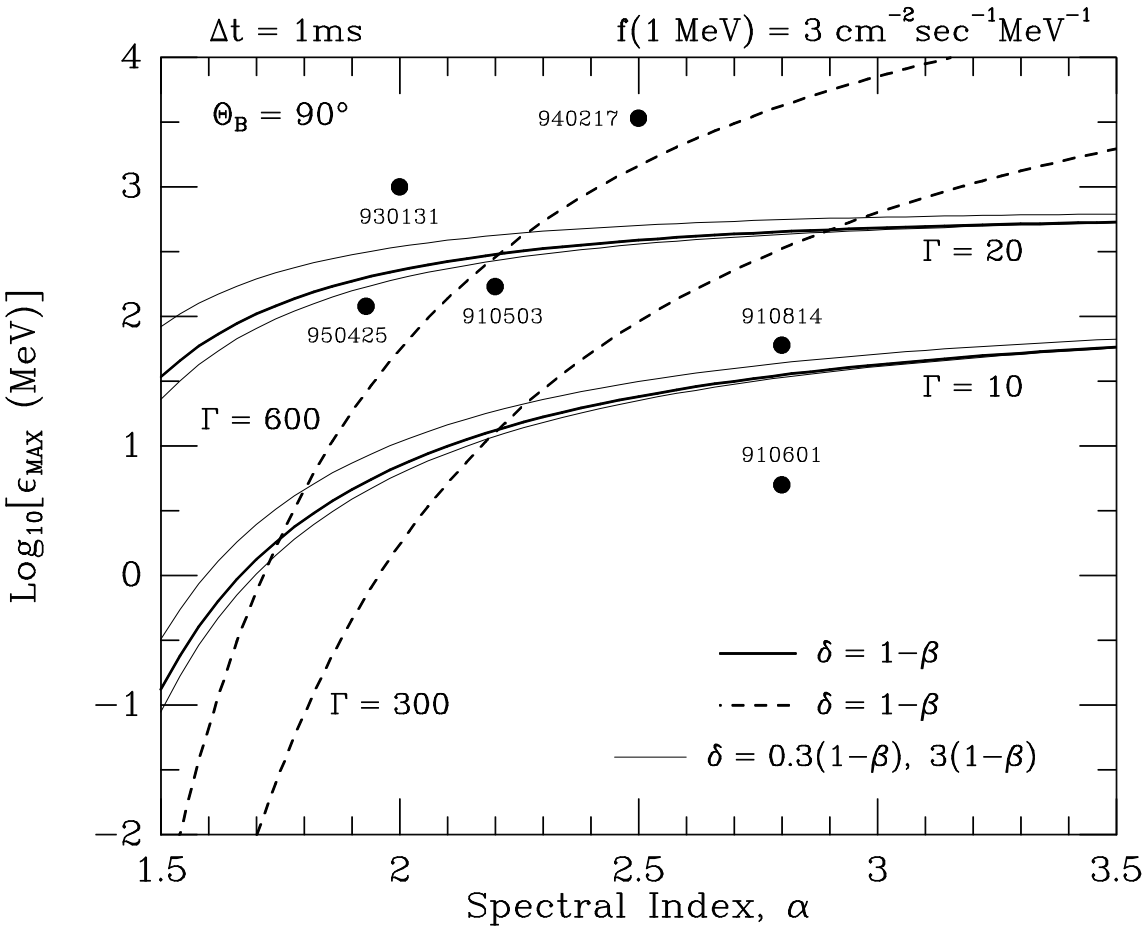

Fig. 6.— The phase space diagram for the observational parameters $\varepsilon_{\rm MAX}$ and α, consisting of contours of constant Γ, as labelled. The contours correspond to solutions of $\tau_{\gamma\gamma} = 1$ for specific choices of Γ $(= \Gamma_{\rm MIN})$ typical of both galactic halo sources at $d = 100\,{\rm kpc}$ (three solid lines for each of $\Gamma = 10, 20$) and cosmological scenarios at $d = 1\,{\rm Gpc}$ (dashed lines: $\Gamma = 300, 600$). The heavy contours represent fractional thicknesses $\delta \equiv \Delta R/R_0 = 1-\beta$, and for the galactic halo cases of $\Gamma = 10, 20$, alternative thicknesses are represented by the light contours, with the lower curves for each Γ denoting $\delta = 0.3(1-\beta)$ and the upper ones $\delta = 3(1-\beta)$. For all contours, the opening angle was set at $\Theta_{\rm B} = 90°$, the variability timescale set at 1 ms, and the flux $f(1\ {\rm MeV})$ at 1 MeV assumed a value typical of EGRET sources. The observed EGRET values of $\varepsilon_{\rm MAX}$ and α for six bursts (see Table 2) are plotted as points; these bursts all have values of $f(1\ {\rm MeV})$ different from the "canonical value" chosen here.

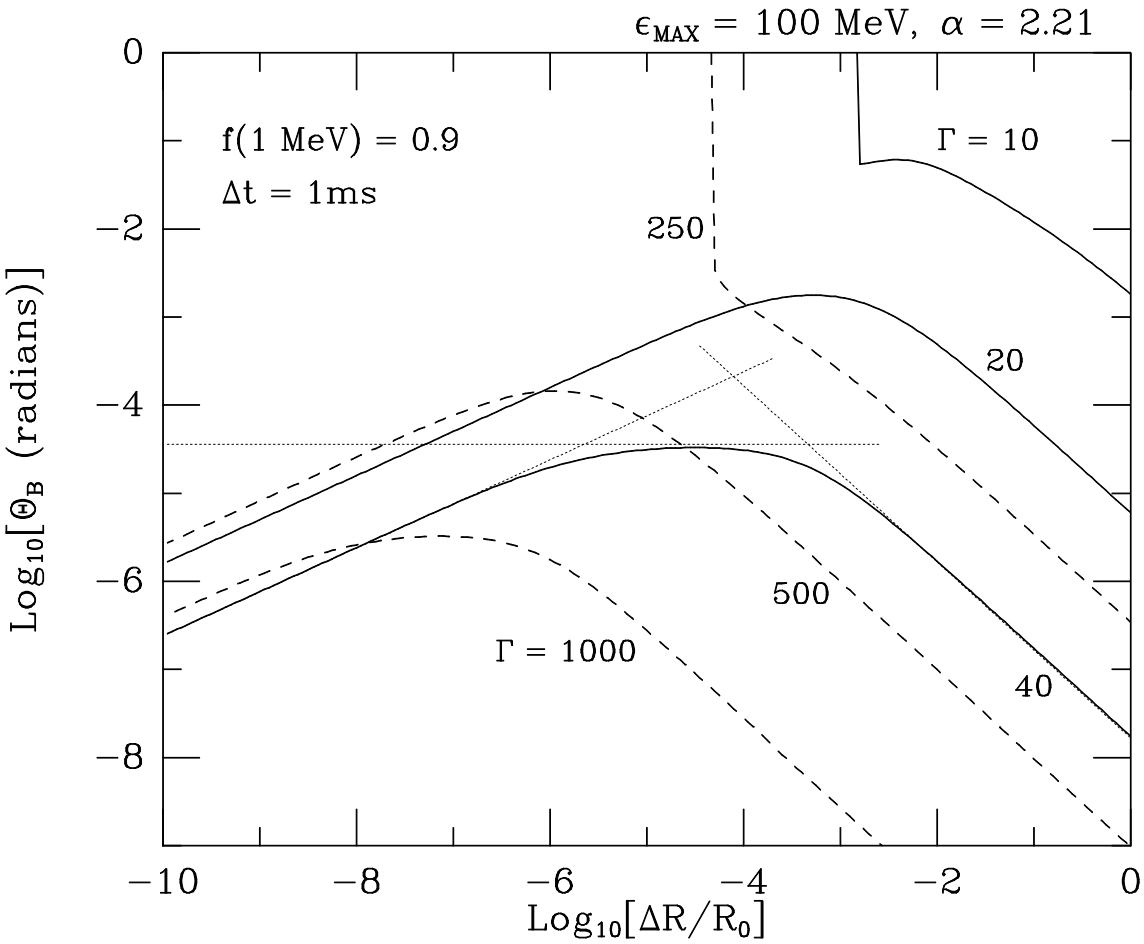

Fig. 7.— The phase space diagram for the theoretical parameters $\Theta_{\rm B}$ and $\delta = \Delta R/R_0$, consisting of contours of constant Γ, as labelled. As in Fig. 6, the contours denote solutions of $\tau_{\gamma\gamma} = 1$ for specific choices of Γ typical of both galactic halo sources at $d = 100\,{\rm kpc}$ (three solid lines with $\Gamma = 10, 20, 40$) and cosmological scenarios at $d = 1\,{\rm Gpc}$ (dashed lines: $\Gamma = 250, 500, 1000$). For all contours, the maximum energy and spectral index were set at $\varepsilon_{\rm MAX} = 100\,{\rm MeV}$ and $\alpha = 2.21$, respectively, and the variability timescale Δt and the flux $f(1\ {\rm MeV})$ at 1 MeV are representative of EGRET-like sources. The vertical portions of the $\Gamma = 10$ and $\Gamma = 250$ contours define thin-shell/thick-shell regimes where the optical depth is independent of $\Theta_{\rm B}$. The three light dotted lines are the asymptotic limits given in Eq. (48).

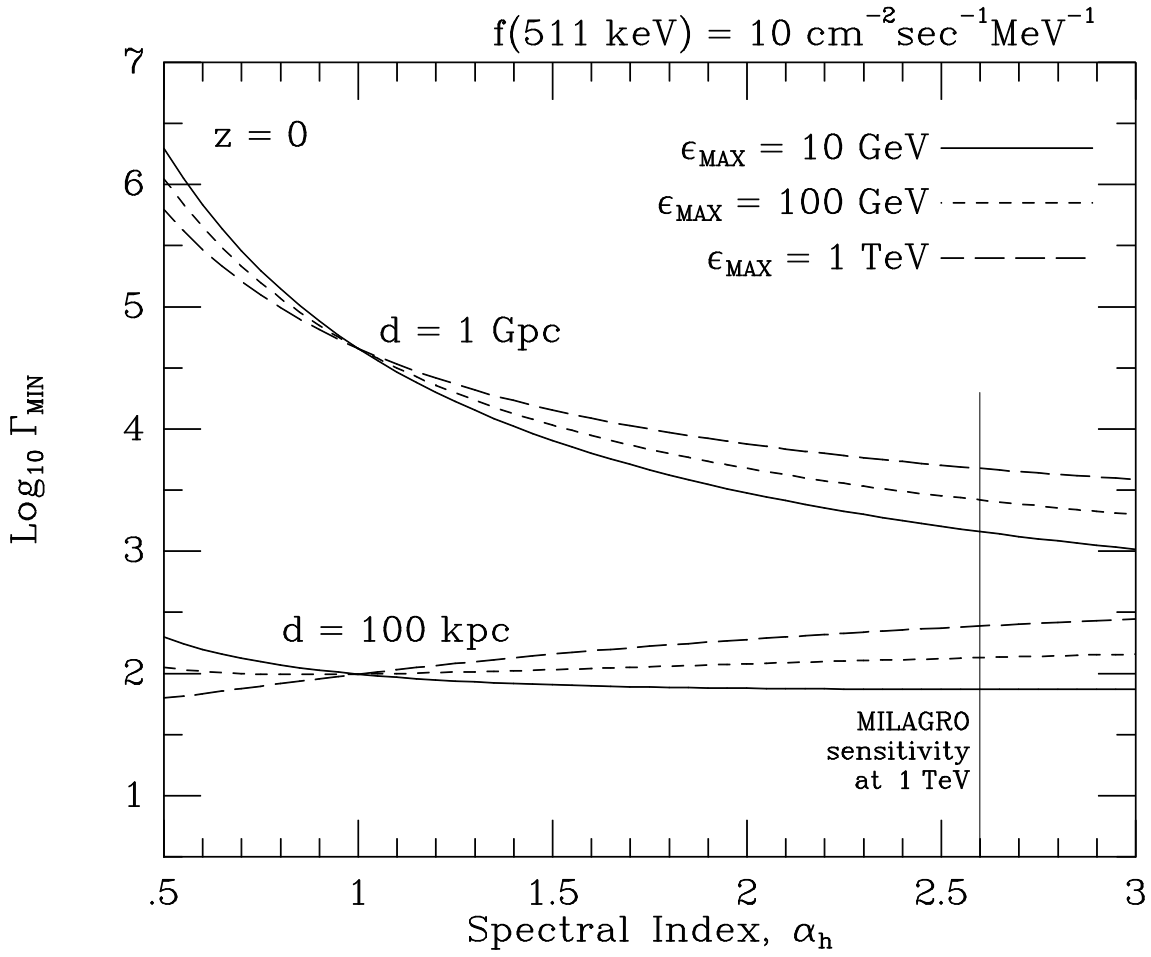

Fig. 8.— Solutions to Eq. (47) for the minimum bulk Lorentz factor $\Gamma_{\rm MIN}$ that guarantees source transparency up to energy $\varepsilon_{\rm MAX}$ for two different source distances d as labelled. Values of $\varepsilon_{\rm MAX}$ are chosen to probe beyond the EGRET energy range up to the domain of air Čerenkov detection techniques. Again infinite power-law source spectra are assumed. The source flux f at 511 keV is typical of BATSE burst detections; for this flux, the MILAGRO experiment will be sensitive to bursts with $\alpha_h \lesssim 2.6$. The cosmological redshift was taken to be $z = 0$ for simplicity.